Iowa Research Online
The University of Iowa's Institutional Repository

University of Iowa
Iowa Research Online

Theses and Dissertations

Spring 2010

Simultaneous automatic detection of optic disc and fovea

Xiayu Xu
University of Iowa

Follow this and additional works at: https://ir.uiowa.edu/etd

 Part of the Biomedical Engineering and Bioengineering Commons

Copyright © 2010 Xiayu Xu

This thesis is available at Iowa Research Online: https://ir.uiowa.edu/etd/630

Recommended Citation

Xu, Xiayu. "Simultaneous automatic detection of optic disc and fovea." MS (Master of Science) thesis, University of Iowa, 2010.
https://doi.org/10.17077/etd.u54qgdib

Follow this and additional works at: https://ir.uiowa.edu/etd

 Part of the Biomedical Engineering and Bioengineering Commons

www.manaraa.com

SIMULTANEOUS AUTOMATIC DETECTION OF OPTIC DISC AND FOVEA

by

Xiayu Xu

A thesis submitted in partial fulfillment of the
requirements for the Master of Science
degree in Biomedical Engineering
in the Graduate College of
The University of Iowa

May, 2010

Thesis Supervisors: Professor Joseph M. Reinhardt
Associate Professor Michael D. Abramoff

www.manaraa.com

Graduate College
The University of Iowa
Iowa City, Iowa

CERTIFICATE OF APPROVAL

MASTER'S THESIS

This is to certify that the Master's thesis of

Xiayu Xu

has been approved by the Examining Committee for the thesis requirement for the Master of Science degree in Biomedical Engineering at the May, 2010 graduation.

Thesis Committee: _____
Joseph M. Reinhardt, Thesis Supervisor

_____
Michael D. Abramoff, Thesis Supervisor

_____
Edwin L. Dove

_____
Mona K. Garvin

_____
Tae-Hong Lim

www.manaraa.com

To My Family

www.manaraa.com

ACKNOWLEDGEMENTS

First of all, I am really grateful to my family for their unconditional support. My father has been such a great model for me. I would like to thank my mother, who is always so supportive in every step in my life.

I wish to express my sincere gratitude to my advisor, Dr. Joseph Reinhardt for his continuous support during my Master's study. Dr. Reinhardt is such a great advisor by always inspiring me with brilliant ideas in my research. He is always there to listen and to give advice. He could notice every small improvement in my study and never hesitate to praise it. His encouragement makes me feel more confident in my study.

I admire Dr. Michael Abramoff, my another advisor greatly. He is really a great mentor who is always enthusiastic on his research area. He brought me to the ophthalmology imaging field that I found to have great interest. He encouraged me to ask questions and to express myself. I could not have come this far without his guidance.

I also thank to the other two committe professors: Dr. Edwin Dove, Dr. Mona Garvin and Dr. Tae-Hong Lim for their advices on the thesis. A special thanks goes to all my fellows in the Ophthalmology research group: Dr. Sangyeol Lee, Dr. Meindert Niemeijer, Dr. Li Tang, Dr. Kyungmoo Lee, Vinayak Joshi, Mark Christopher and Qiao Hu. Thanks for all the great ideas and advices from them. I really enjoyed the discussions between all of us.

During the past two years, I have had a great time with my labmates in the Medical Imaging Research Lab. I would like to thank Kai Ding, Panfang Hua,

www.manaraa.com

Vinayak Joshi, Tarunashree Yavarna and Kaifang Du. They are the first ones I can turn to when I have troubles in research, in study and even in daily life. Thanks to them for their help and being fun to be with. As a senior student, Kai has given me lots of help in research as well as in life. Here I would like to give my sincere thanks to him.

Again, I would like to give my thanks to all the people who helped me in the past years.

www.manaraa.com

TABLE OF CONTENTS

www.manaraa.com

www.manaraa.com

LIST OF TABLES

Table

www.manaraa.com

LIST OF FIGURES

Figure

www.manaraa.com

www.manaraa.com

www.manaraa.com

www.manaraa.com

CHAPTER 1
INTRODUCTION

Early diagnosis and treatment of various eye diseases is very important to prevent it from getting worse or even leading to blindness. For example, if diabetic retinopathy is successfully diagnosed in an early stage, it can be treated by laser surgery and strict glucose control. However, if the diseases has already caused vision loss, visual acuity usually cannot be restored.

Conventional approaches for early diagnosis of diabetic retinopathy incorporate a dilated fundus exam by an ophthalmologist utilizing a slit-lamp biomicroscope [17]. This is a very inefficient approach that not only waste ophthalmologist's time, but also expensive for the patients. Efforts to increase the efficiency of diabetic retinopathy screening have focused on the use of fundus photographs.

Fundus photography is the preferred medium for large scale screening [15]. Digital fundus photography allows instantaneous examination of the retina when necessary, quick storage and access of the images. The images can be acquired anywhere, but read at a central specialized institution. However, there are more than 18 million people with diabetes in the United State as of year 2005. The regular dilated fundus examination is recommended once a year and there are normally four fundus images in one examination. So the image data is huge. Moreover, only 10% or less of these patients may have diabetic retinopathy, meaning about 90% of the images are normal [5]. So computer aided diagnosis (CAD) is necessary. CAD interprets and analyzes all images of a patient. If abnormalities exist, the case is further examined by an ophthalmologist. Otherwise it is stored without further examination.

www.manaraa.com

An essential processing step in an automatic diabetic retinopathy screening system is detection of the position of the anatomy. This is important for two reasons. First, it is often necessary to mask out the normal anatomy before finding abnormal structures. For instance, the optic disc might be mistaken as bright lesion if it is not masked out. Secondly, the distribution of of the abnormalities is not uniform. Certain types of abnormalities occur more often in specific areas on the retina. So if we have the location of the anatomy, the position of a lesion relative to the major anatomy could thus be useful as a feature for later analysis and classification of pathologies [15].

There are three major anatomical structures in color fundus photographs, the optic disc, the fovea, and blood vessels. Some work has been reported in optic disc detection or fovea detection [6] [8] [9] [10] [11] [13] [19] [20]. Most optic disc detection methods are based on the fact that the optic disc is the convergence point of blood vessels and it is normally the brightest structure on the image, while most fovea detection methods depend partially on the result of optic disc detection. Further discussion of previous work is given in Section 2.4.

Here we propose a method that can automatically detect the optic disc and fovea simultaneously, and the detection result of one structure can facilitate detection of the other structure. First, a set of features are extracted from the image and a k-nearest-neighbor regression is used to give every pixel a soft label that indicate the likelihood of that pixel being a part of the optic disc or fovea. Then, a second set of features are extracted from the likelihood image that uses the mutual information between the optic disc and fovea. The detection result of the first k-nearest-neighbor regression is enhanced during a second k-nearest-neighbor regression. Finally, the

www.manaraa.com

pixels with the highest likelihood of being an optic disc center and a fovea center are selected.

www.manaraa.com

CHAPTER 2
BACKGROUND AND PREVIOUS WORK

2.1 Eye Anatomy

The human eye is a complex biological device. The mechanism of a camera is often compared with the working of the eye, as shown in Fig. 2.2. Light entering the eye is first refracted when it passes through the cornea. It then passes through the pupil and is further refracted by the lens. Finally, it reaches the retina and is converted to electrical signals by photosensitive photoreceptor. The electrical signals are transmitted to the brain along the optic nerve [18].

The cornea is the transparent front part of the eye. It is the first structure that is able to refract the light entering the eye. However, the focal distance of the cornea is fixed, which means that the cornea can only refract light with a constant angle.

The lens, on the other hand, can adjust its focal distance so that incoming light can be focused on the retina. This is similar to the focusing of a photographic camera via movement of its lenses. The lens is a transparent structure lying behind the iris and the pupil.

The iris is a membrane organ in the eye. It controls the diameter and size of the pupil and hence the amount of light reaching the retina. The movement of iris is controlled by the iris dilator muscle. The pupil is an opening in the center of the iris. It allows light to enter the eye and reaches the lens. The pupil appears to be black because most of the light entering the pupil is absorbed.

The vitreous is the transparent, colorless, gelatinous mass that fills the space

www.manaraa.com

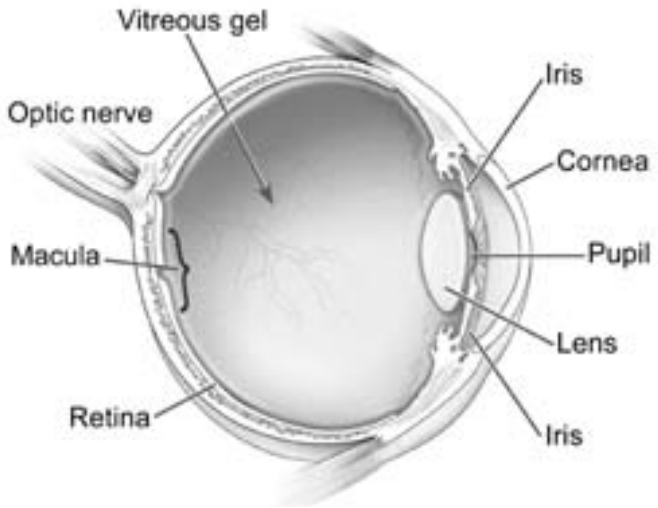

Figure 2.1: Simple illustration of eye anatomy (Fig from [7]).

between the lens and the retina. It is also referred to as the vitreous body or vitreous humor. The vitreous contains very few cells, no blood vessels, and $98-99\%$ of its volume is water. Unlike the fluid in the frontal part of the eye which is continuously replenished, the gel in the vitreous is stagnant. So if blood or cytosol get into the vitreous, they may not be reabsorbed for an extended period of time. A vitreous hemorrhage is a typical symptom of diabetic retinopathy (see Section 2.2).

The optic disc or optic nerve head is the location where ganglion cell axons exit the eye. The optic nerve is a bundle of more than one million nerve fibers. The optic nerve connects the retina to the brain. It is also the place where all retinal blood vessels originate and converge. The optic disc is placed 3-4mm to the nasal side of the fovea.

The retina is a light sensitive tissue layer lining the inner surface of the eye. The photosensitive cells on the retina detect light passing through the cornea and lens. The retina is comparable to the film of a camera.

www.manaraa.com

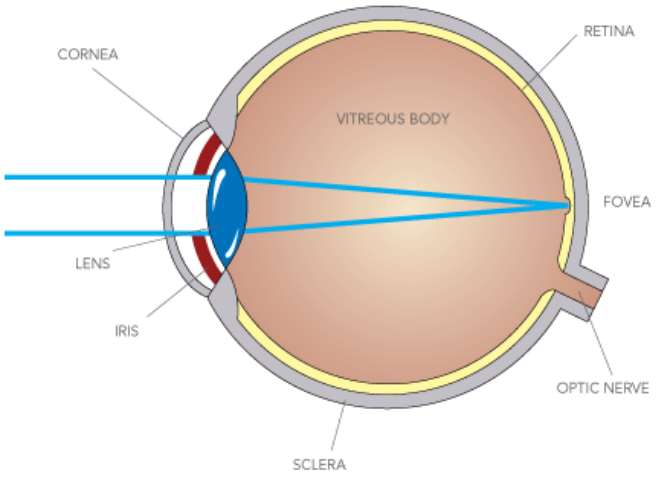

Figure 2.2: Light path of the visual system (Fig from [4]).

The fovea centralis, usually known as the fovea, is located in the center of the macula region on the retina(as shown in Fig. 2.1). The fovea is responsible for sharp central vision. Approximately 50% of the nerve fibers in the optic nerve carry information from the fovea [18].

2.2 Common Eye Diseases

Diabetic retinopathy refers to the damage of the blood vessels in the retina as a complication of diabetes. Diabetic retinopathy is the most common diabetic eye disease and the primary cause of blindness in American working population.It causes more than 24000 new cases of blindness each year [5]. Diabetes disrupts the glucose balance in the blood over time. This high blood glucose can damage blood vessels in the retina, and cause retinal ischemia. Eventually, new blood vessels start to grow and retinal vessels start to leak. The smallest blood vessels are damaged first. These new blood vessels are very weak. They break easily and can detach the retina. A regular dilated eye exam has been shown to prevent blindness and visual

www.manaraa.com

loss in patients with diabetes.

A Cataract is the clouding of the lens in the eye that affects vision. Most cataracts are related to aging. As people age, some of the protein inside the lens may clump together and opacity. Those cloudy areas prohibit the light from reaching the photosensitive cells, which results in a incomplete image on the retina. Diabetes, smoking, alcohol and prolonged exposure to sunlight are factors that believed to increase people's risk of developing a cataract [2].

Glaucoma is a group of diseases that damage the optic nerve and may result in vision loss and blindness. Glaucoma occurs when the normal fluid pressure inside the eye increases. Open-angle glaucoma is the most common form. Early symptoms of glaucoma may include peripheral vision loss, which means they may miss objects to the side and out of the corner of their eye. Without treatment, people will slowly lose their peripheral vision. African Americans over age 40, everyone over age 60, and people with a family history of the disease are at a higher risk of developing glaucoma [3]. However, with early treatment, a visual loss is usually avoidable.

2.3 Fundus Photograph

The fundus of the eye is the interior surface of the eye, including the retina, optic disc, macula and fovea. The fundus is the only part of the human body where both the circulation and the nerve tissue can be observed directly. A fundus photograph is an image of the fundus taken by an ophthalmoscope, or a fundus camera, which is designed to photograph the interior surface of the eye, including the retina, optic disc, and macula. Fundus photographs are usually taken in screening programs, where the photos can be analyzed later for diagnosis and be used to monitor the

www.manaraa.com

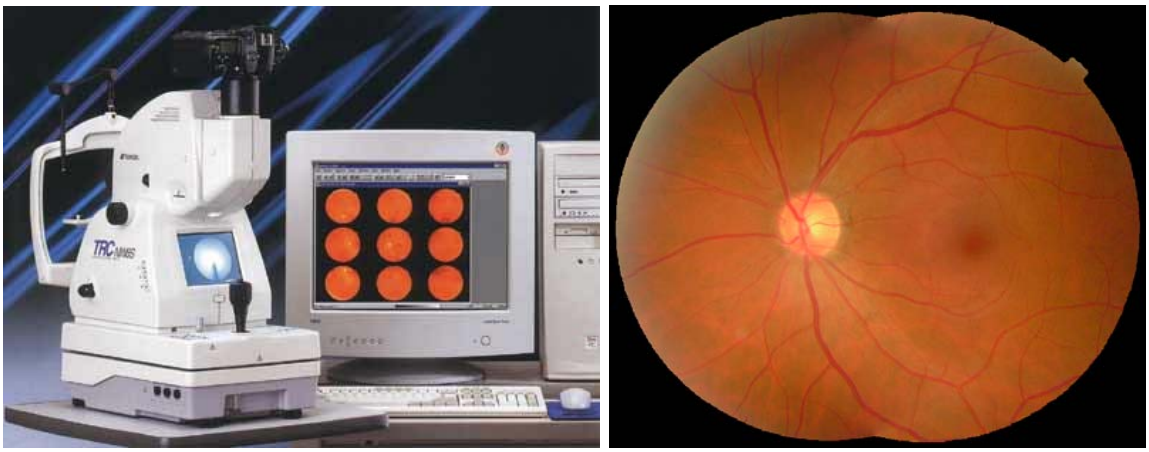

(a) (b)

Figure 2.3: Fundus camera and fundus photograph. (a)Fundus Camera (Fig from [1]). (b)A Normal Eye Fundus Photograph.

progress in many eye diseases. A normal human fundus photograph is shown in Fig. 2.3.

A normal human fundus photograph is reddish. Three major structures are presented in a normal human eye fundus photograph, the optic disc (or optic nerve head), the macula and blood vessels. The optic disc appears to be a bright region in the image, where all blood vessels converge. Arteries are brighter comparing with veins. The macula is a dark region where few blood vessels present. Medical signs, such as hemorrhages, exudates, cotton wool spots, blood vessel abnormalities, and pigmentation can be detected using fundus photographs.

In a screening project, where thousands of fundus photographs need to be examined, automatic detection of the structures and abnormalities is important. In this work, we propose an automatic and simultaneous method to detect the optic disc and fovea.

www.manaraa.com

2.4 Previous Work

Many techniques have been proposed to automatically detect the optic disc, fovea or both. Most optic disc detection methods are based on the fact that the optic disc is usually the convergence point of blood vessels and that it is the brightest region in a fundus photograph. Hoover et al. proposed a method for optic disc detection based on the combination of vessel structure and pixel brightness [9]. If strong vessel converge point is found in the image, it is regarded as the optic disc. Otherwise the brightest region is detected. They reported a 88.9% (72/81) correctness of which 50 images showed disease. Foracchia et al. proposed a optic disc detection method based on vessel directions [8]. A parabolic model of the main vascular arches is established and the model parameters are the directions associated with different locations on the parabolic model. The point with a minimum sum of square error is reported as the optic disc location. Other optic disc detection methods also used the optic disc brightness information. The optic disc was successfully located in 97.5% of the images. In Lowell et al. by matching an optic disc model using the Pearson correlation, an initial optic disc location is determined [11]. This stage was reported a 96.7% (87/90) correct rate. Then a deformable contour model was used to trace the optic disc boundary.

Compared with the automatic detection of optic disc, less work has been done in the field of fovea detection. Most methods use the fact that the fovea is a dark region in the image and that it normally lies in a specific location relative to the optic disc and main vascular arch. In Fleming, approximate locations of the optic disc and fovea are obtained using the elliptical form of the main vascular arch [6]. Then the locations are refined based on the circular edge of the optic disc and the local darkness

www.manaraa.com

at the fovea. Positional accuracy for optic disc is 98.4% and 96.5% for fovea. Li and Chutatape also proposed a method to select the brightest 1% pixels in a gray level image [10]. Then the pixels are clustered and principal component analysis based on a trained system is applied to extract a single point as the estimated location of optic disc. A fovea candidate region is then selected based on the optic disc location and the main vascular arch shape. Within the candidate region, the centroid of the cluster with the lowest mean intensity and pixels number greater then 1/6 disk area is regarded as fovea location. A correct rate of 98.9% (88/89) for the optic disc and 100% (35/35) for the fovea is reported. In Sinthanayothin's paper, the optic disc were located as the area with the highest variation in intensity of adjacent pixels. While the fovea were extracted using intensity information and a relatively distance to the optic disc [19]. 99.1% (111/112) optic disc locations are successfully detected. The fovea is correctly detected on 84.5% (60/71) of images showing the complete fovea, and 62.1% (18/29) of images showing more than half of the fovea on image boundary. Tobin et al. proposed a method to detect the optic nerve head based on blood vessel features, such as density, average thickness and orientation [20]. Then a fovea location is determined based on the location of optic disc and a geometry model of main blood vessels. Niemeijer et al. proposed a method to automatically localize both the optic disc and fovea in 2008 [13]. For the optic disc detection, a set of features are extracted from the color fundus image. A k-nearest-neighbor classification is used to give a soft label to each pixel on the test image. The probability image is blurred and the pixel with the highest probability is detected as optic disc. The detection of the fovea is associated with the detection of the optic disc. A relative position information between the optic disc and the fovea is used to limit the search of fovea into a certain

www.manaraa.com

region. For each possible location of the optic disc, a possible location of the fovea is given. The possible locations for the fovea is stored in a separate image and the highest probability location is detected as the fovea location. The method proposed in this thesis is an extension of the work of Niemeijer et al.

www.manaraa.com

CHAPTER 3
METHODOLOGY

Here we propose a method that can detect the optic disc and fovea simultaneously. This new method is an extension of the work of Niemeijer et al [13]. Figure 3.1 describes the overall method in this work. The input is the color fundus image. The green, red and blue channel are split and a set of features are extracted from them separately. Similarly, features are extracted from the vessel segmentation image and the distance transform of the vessel segmentation image. These features are sent to the k-nearest-neighbor (k-NN) classifier. The output of the k-NN classifier is a probability map with each pixel labeled a probability of within an optic disc or a fovea. The probability image is thresholded into an optic disc probability image and a fovea probability using a different threshold. Then another set of features are extracted from these images separately and sent to the k-NN classifier. A second probability image is generated. The first probability image and the second probability image are added together as the final output.

Image preprocessing methods is described in section 3.1. Feature extraction and feature selection are shown in section 3.2 and 3.3. Section 3.4 describes how the first k-NN classification is implemented. At last, the second stage k-NN classification is shown in section 3.5.

www.manaraa.com

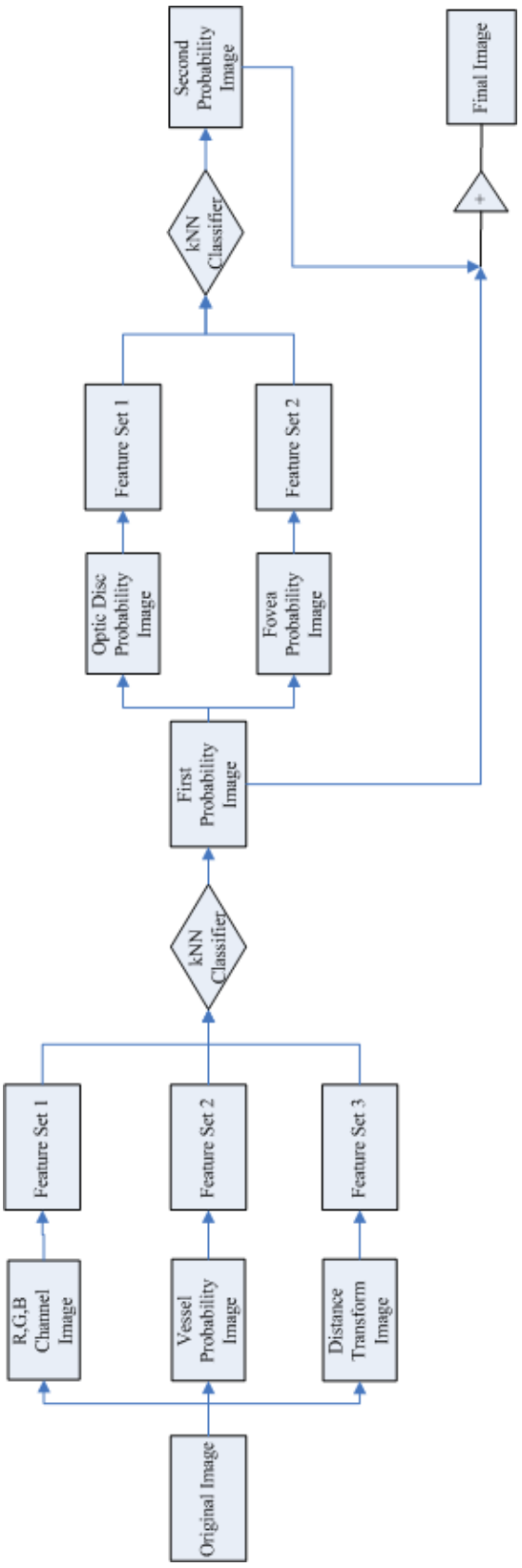

Figure 3.1: A flow chart of the method.

www.manaraa.com

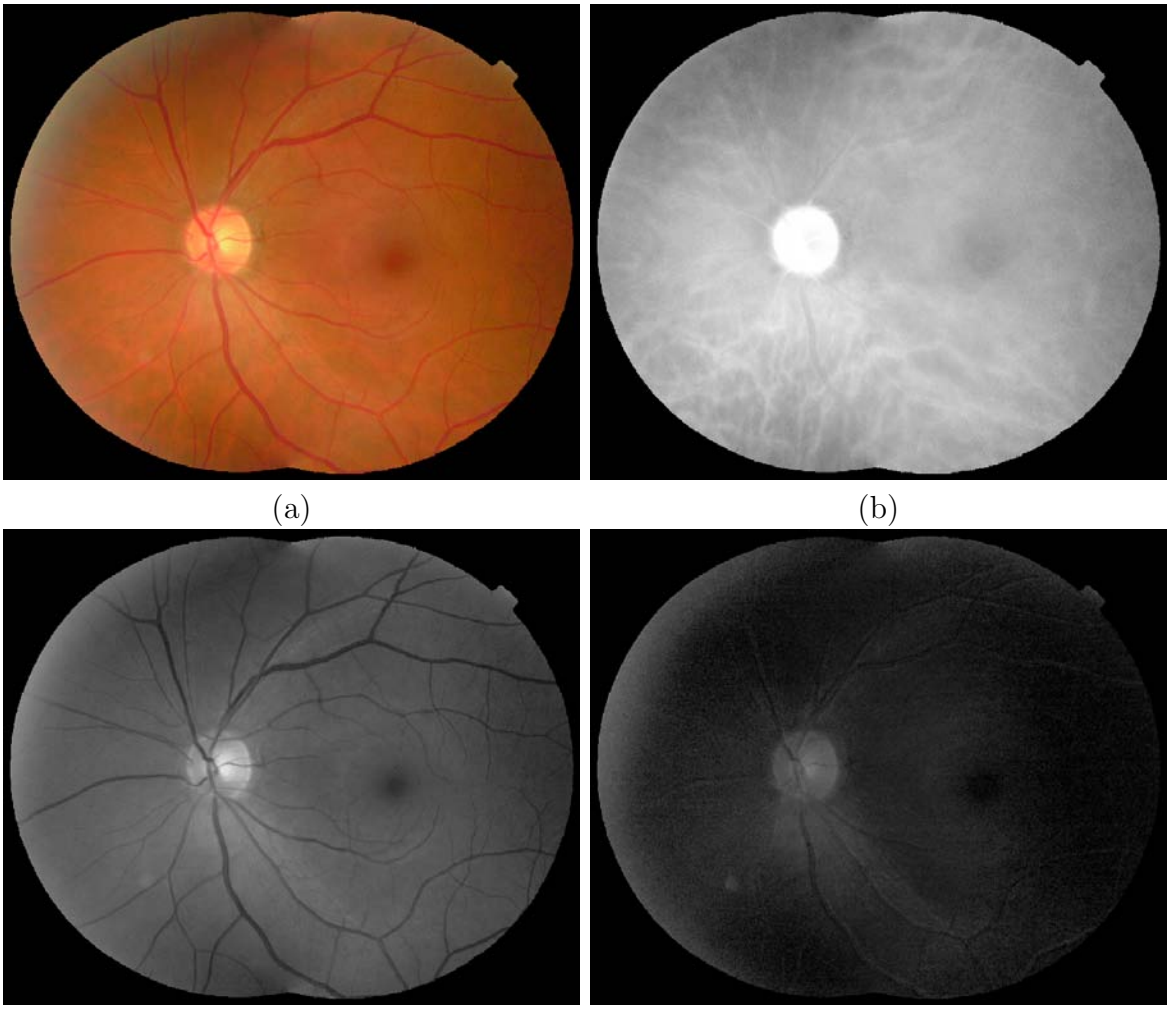

(a) (b)

(c) (d)

Figure 3.2: RGB channels of Fig 2.3. (a)Color fundus image. (b)Red channel. (c)Green channel. (d)Blue channel.

3.1 Image Pre-processing

3.1.1 RGB Channels

In order to extract the intensity information from different color channels, the red, green and blue channels are extracted from the color fundus image (Fig. 3.2). The green component allows the best contrast between retinal vessels and background. The red channel is usually saturated while the blue component is very dark and contains lots of noise. We extract features from all three channels and let

www.manaraa.com

the feature selection decide which features are useful (see Section 3.3).

3.1.2 Blood Vessel Segmentation

As mentioned in Section 2.1, the optic disc is the convergence point of blood vessels. The fovea center has very few blood vessels. Consequently, blood vessel features such as vessel width, orientation, etc. can be used as indicator of the optic disc and fovea positions. In order to measure vessel features, a vascular segmentation is required. We applied the vessel segmentation method proposed by Niemeijer et al [14]. This segmentation method is trained using a set of images in which all vasculature has been manually segmented. A posterior probability map was produced with each pixel's gray value being the probability of this pixel being a vessel pixel. An example of the probability image is shown in Fig. 3.3.

3.1.3 Vessel Centerline Image

The probability image is then thresholded to generate a binary vessel segmentation image. The threshold is set to 110 in this study so that big blood vessels can be maintained while small branches and noise are discarded. In the binary vessel image, a pixel value of 255 indicates that it is a vessel pixel while 0 indicates it is a background pixel.

The centerlines of blood vessels are extracted from this binary image through sequential thinning approach [12]. The structuring element E and L used in sequential thinning are shown in Equations 3.1 and 3.2. $*$ means the pixel at that position can be either 0 or 1. The other five elements are given by rotation.

www.manaraa.com

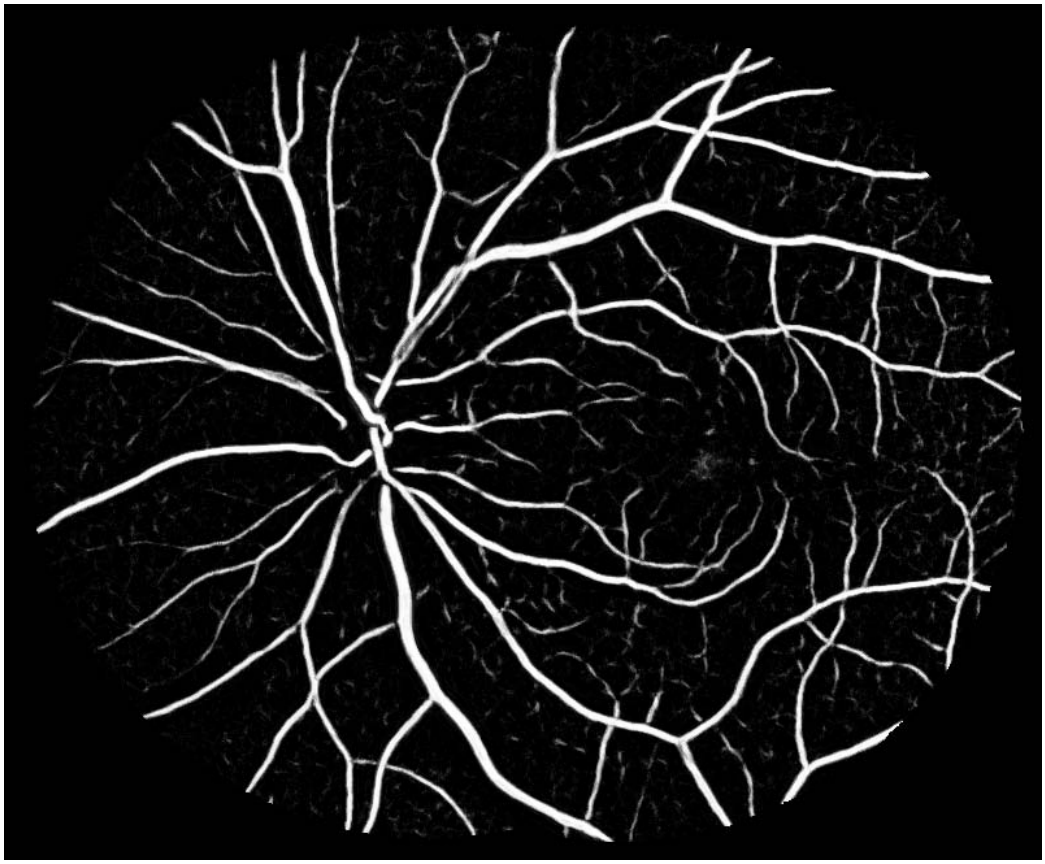

(a)

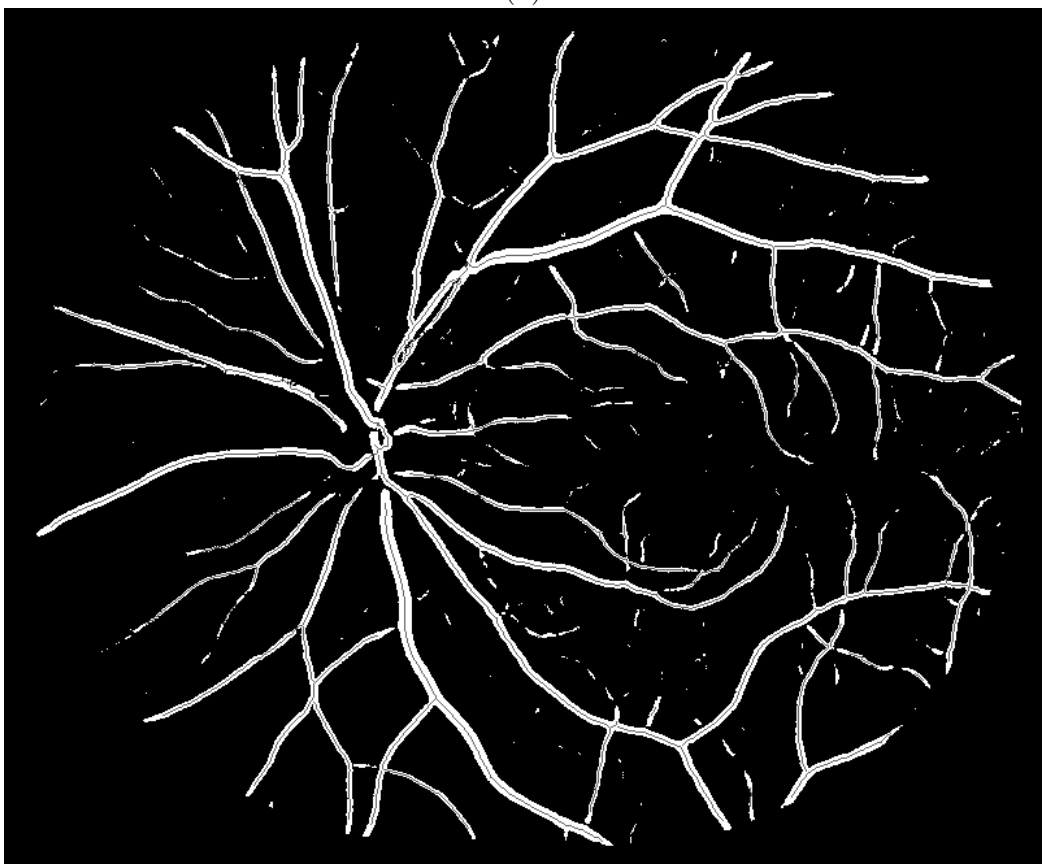

(b)

Figure 3.3: Vessel probability image and vessel centerline image of Fig 2.3. (a)The vessel probability image. (b)The final binary image with centerline pixel inside.

www.manaraa.com

$$E_1 = \begin{bmatrix} * & 1 & * \\ 0 & 1 & 0 \\ 0 & 0 & 0 \end{bmatrix}, \quad E_2 = \begin{bmatrix} 0 & * & * \\ 0 & 1 & 0 \\ 0 & 0 & 0 \end{bmatrix}, \cdots, \quad E_7 = \begin{bmatrix} * & 0 & 0 \\ * & 1 & 0 \\ 0 & 0 & 0 \end{bmatrix} \tag{3.1}$$

$$L_1 = \begin{bmatrix} 0 & 0 & 0 \\ * & 1 & * \\ 1 & 1 & 1 \end{bmatrix}, \quad L_2 = \begin{bmatrix} * & 0 & 0 \\ 1 & 1 & 0 \\ * & 1 & * \end{bmatrix}, \cdots, \quad L_7 = \begin{bmatrix} 0 & 0 & * \\ 0 & 1 & 1 \\ * & 1 & * \end{bmatrix} \tag{3.2}$$

Sequential thinning is defined as Equation 3.3. Let $B_{(1)}, B_{(2)}, ..., B(n)$ denote the structuring elements E and L mentioned above. $X \ominus B$ means erode X with element B. $X \ominus B = \{p \in \varepsilon^2 : p = x + b \in X \ for \ every \ b \in B\}$.

$$X \ominus B_{(i)} = (((X \ominus B_{(1)}) \ominus B_{(2)}) ... \ominus B_{(n)}) \tag{3.3}$$

The centerline image are then added back to the binary image and gives a gray value of 100, in order to distinguish from the vessel pixels, which is 255. An example image is shown in Fig. 3.3.

3.1.4 Distance Transform

As mentioned, usually no blood vessel can be observed around the fovea, while lots of vessels are around the optic disc since it is the convergence point of blood vessel. Therefore, a distance transform of the binary vessel segmentation image is generated

www.manaraa.com

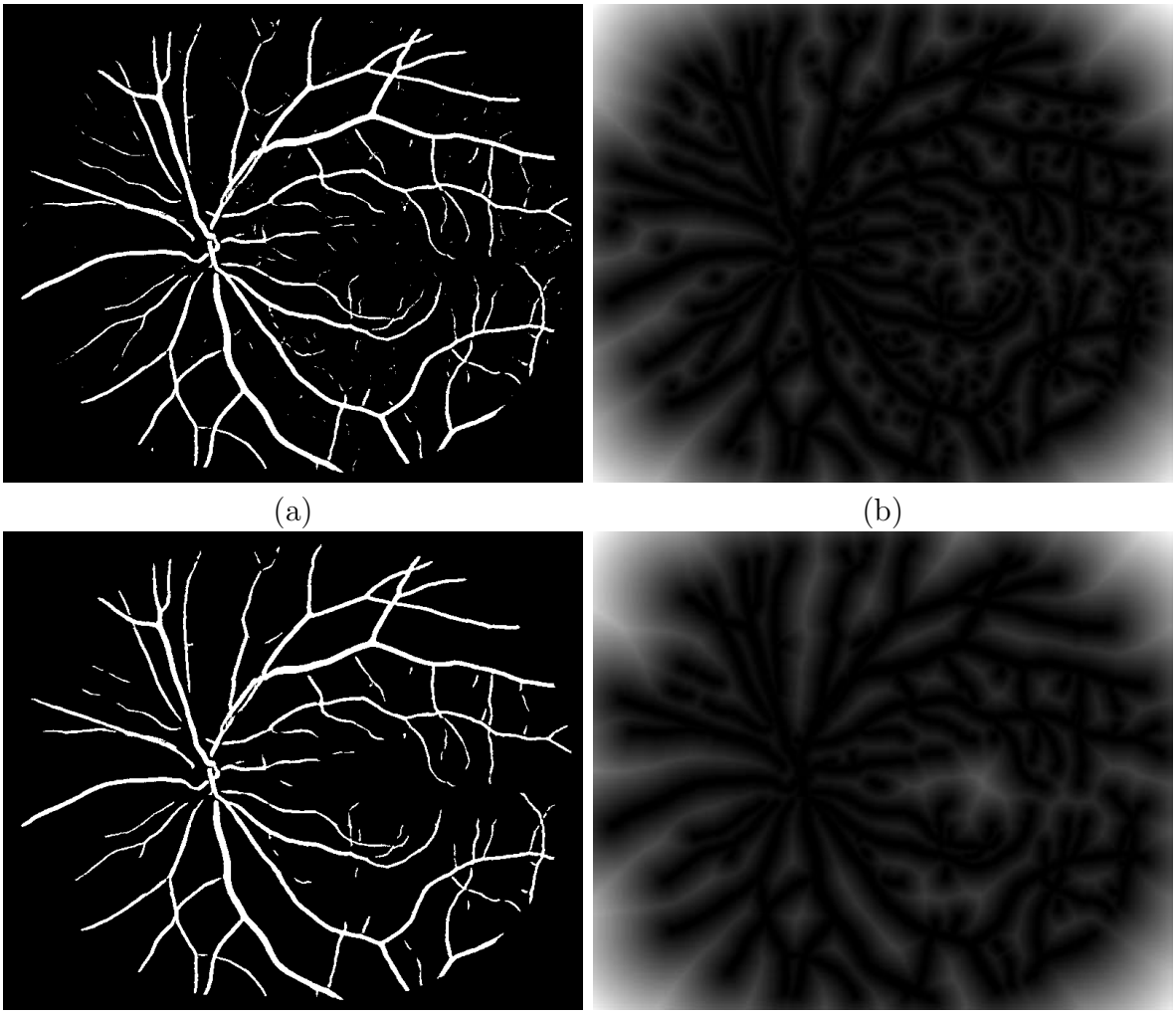

Figure 3.4: Distance transform of Fig 2.3. (a)The binary image before erasing noise regions. (b)The distance map of (a). It is influenced by small noises greatly. (c)The binary image after erasing noise regions. (d)The distance map of (c). The influence by noise regions disappears.

to make use of this observation (see Fig. 3.4). The brightness of a pixel denotes its distance to the nearest blood vessel pixel. So the blood vessel pixels have a brightness 0 because it has a distance 0 to blood vessel. The optic disc region normally has a very low average brightness, because of a high blood vessel density. The four corners and the fovea region are usually much brighter because of the absence of vessel pixels.

However, if we use the binary image directly to generate the distance image,

www.manaraa.com

the distance map will be influenced by small noise, as shown in Fig. 3.4 (a) and (b). If there are small noises around the fovea, the distance image will be changed greatly. In order to solve this problem, the vessel regions that have an area smaller than 20 pixels are erased from the binary blood vessel image. As shown in Fig. 3.4 (c) and (d).

3.2 Feature Extraction

For each sample point, a set of features are extracted from the pre-processed images (see Section 3.1). A circular template is used to extract those features (see Fig. 3.5). The outer diameter $\mathcal{R}$ is set to 50 pixels because it is comparable to the diameters of the optic disc and fovea. The inner diameter r of the template is designed to best obtain the intensity contract between the center of the fovea and the peripheral. In our study, we empirically chose the inner radius 25 pixels. Since the optic disc is the entry point for the optic nerve, for pixels around the optic disc, all the vessel segments should oriented to the template center. Also, despite the few numbers, the vessels that approach the fovea center from the top and bottom directions are expected to be more or less parallel to the y-axis, while the vessels approaching from the left and right should approximately be parallel with the x-axis. Based on this observations, the template is also divided into four quadrants, in order to better capture the vessel orientation differences in different directions.

The features extracted from the pre-processed images are shown in Table 3.2. Among these features, feature 1-30 is extracted from the vessel probability map. Feature 31-42 are extracted from the red, green and blue channel. Feature 43-45 are from the distance transform image of the binary image.

www.manaraa.com

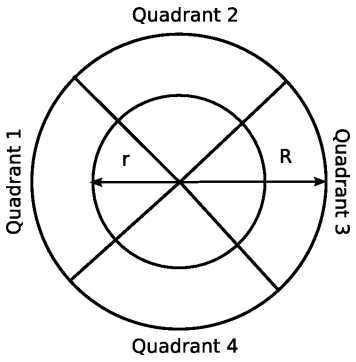

Figure 3.5: Circular template of inner radius r and outer radius $\mathcal{R}$. The template is divided into four quadrants.

3.2.1 Features from Vessel Image

Figure 3.6 shows an simple illustration of how the vessel features are calculated within the template. The template radius is 15 pixels. The inner template boundary is not shown because it is not used in vessel feature extraction. Pixel 1 denotes the template center.

Under each quadrant, the number of vessels is the number of vessel pixels under the quadrant. So the number of vessels for quadrant 1 is 27. Similarly, vessel number for quadrant 2, 3, and 4 is 39, 41 and 0 separately.

For each centerline pixel p, the three neighbor centerline pixels in the left and in the right are found. So a vessel centerline segment of length 7 is selected. Near the end of the vessel, where less than three neighbors can be found at one end, only centerline coordinates inside the vessel are used, 4 pixels for the end point. If the total length of the centerline segment is less than 4 pixels, it is regarded as noise and discarded. For example, the 6 neighbors for pixel 2 are labeled red in Fig. 3.6.

For this centerline segment, principal component analysis is applied to find the dominant orientation. The orientation is regarded as the orientation of centerline

www.manaraa.com

Table 3.1: Features extracted for the first k-NN classification.

feature #	feature description	template	image
1-4	number of vessels	quadrants	vessel image
5-8	average vessel width	quadrants	vessel image
9-12	standard deviation of vessel width	quadrants	vessel image
13-16	average vessel orientation difference	quadrants	vessel image
17-20	standard deviation of vessel orientation difference	quadrants	vessel image
21-24	maximum vessel width	quadrants	vessel image
25-28	orientation difference of max-width vessel	quadrants	vessel image
29	vessel density	whole template	vessel image
30	average vessel width	whole template	vessel image
31-36	average image intensity	inner/outer template	R,G,B image
37-42	standard deviation of image intensity	inner/outer template	R,G,B image
43-44	average distance to vessel pixel	inner/outer template	distance image
45	maximum distance to nearest vessel pixel	inner template	distance image

pixel p. In this example, the first principal component for the vessel segment centered at pixel 2 is $[0.707, 0.707]$, as shown in arrow a. The vessel angle is 45 degrees.

The vessel width at pixel p is measured along a line perpendicular to the dominant vessel orientation. In Fig. 3.6, the vessel width is measured along arrow b. The vessel width at pixel 2 is two pixels.

After the vessel width and orientation is computed for each centerline pixel, the width average, width standard deviation, orientation average, orientation standard deviation and maximum vessel width can be calculated consequently.

$$\bar{x} = \frac{\sum_{i=1}^{n} x_i}{n} \tag{3.4}$$

www.manaraa.com

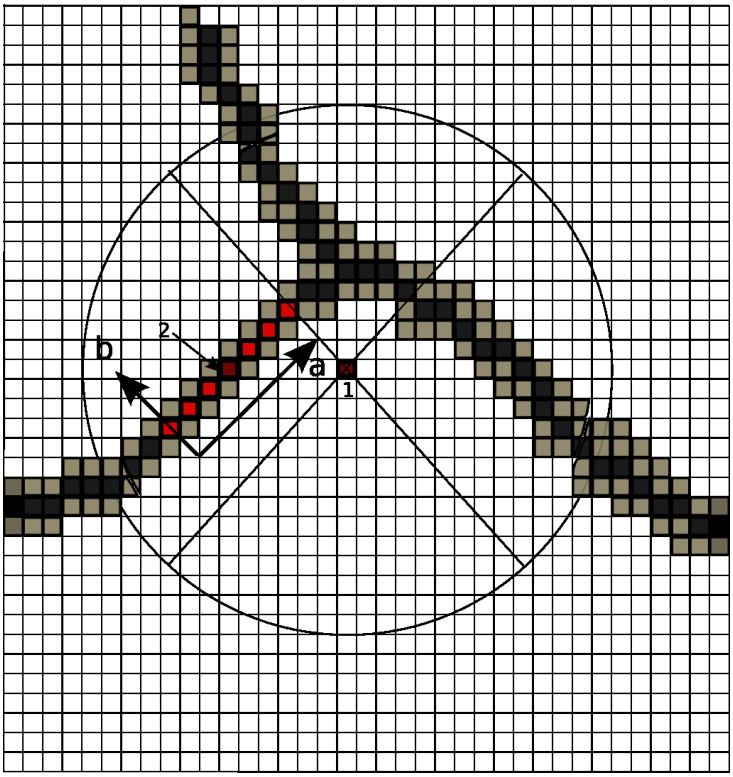

Figure 3.6: An illustration of how vessel features are computed. The outer radius of the template is 15 pixels. The inner radius is not shown because it is not used in vessel feature extraction. Vessel pixels are shown in gray and vessel centerlines are shown in black. Pixel 1 is the template center. Arrow a denotes the vessel orientation at pixel2. Arrow b denotes the direction along which the vessel width is calculated.

$$s = \sqrt{\frac{1}{n-1}\sum_{i=1}^{n}(x-\bar{x})^2} \tag{3.5}$$

The vessel density under the complete template is measured by dividing the number of vessel pixels under the whole template by the area of the template. In the example shown in Fig. 3.6, the total number of vessel pixels within the whole template is 107. The template area is $\pi\mathcal{R}^2 = 706$ pixels. So the vessel density is $107/706 = 0.15$.

The average vessel width under the whole template is calculated by dividing the number of vessel pixels by the number of centerline pixels. So in this example

www.manaraa.com

it is 107 divided by 34, which is 3.4. So the average vessel width is 3.4 within this template.

3.2.2 Features from RGB Image

The average and standard deviation of pixel intensities within the inner template and outer template are extracted separately on the red, green, and blue channels. The outer template radius $\mathcal{R}$ is set to 50, which is comparable to the radius of optic disc and fovea. Hence, if the template is centered around optic disc, the average intensity should be high while the standard deviation is supposed to be low, because of the low dispersion of image intensity. Similarly, around fovea, the average image intensity should be low and the standard deviation of intensity should also be low. Especially on the green channel, where optic disc, fovea, and blood vessels all have the best contract with the background. On the red channel, which is usually over saturated, the overall brightness is very high, often not only for the optic disc region; while on the blue channel, the overall brightness is usually very low, not only for the fovea region. But we still compute all those features and let the feature selection to decide which ones are useful (see Section 3.3). The equations for average and standard deviation is given in equation 3.4 and 3.5.

In this study, the radius of the inner template r is set to 25 pixels, because it gives a good intensity contract between the inner template and outer template when the template is centered around fovea.

3.2.3 Features from Distance Image

The average distance to the nearest vessel pixel for both inner and outer templates are extracted from the distance image. On the distance image, the distance

www.manaraa.com

to the nearest vessel pixel is simply the pixel intensity (see Section 3.1). Near the optic disc, the distance image is usually very dark because of the high vessel density, while near the fovea and four corners of the image, the distance image is usually very bright because of the absence of blood vessel.

3.2.4 Dependent Variable $\mathcal{D}$

In order to build a relationship between those features from sampling points with the true distance to optic disc and fovea, a distance variable $\mathcal{D}$ must be defined. First of all, for each sample pixel, the Euclidean distance to optic disc d_{od} and fovea d_f is calculated separately. Then dependent variable $\mathcal{D}$ is defined as follows:

$$\mathcal{D} = \begin{cases} d_f & \text{if} \quad d_f < R \\ 2R - d_{od} & \text{if} \quad d_{od} < R \\ R & \text{otherwise} \end{cases} \tag{3.6}$$

Parameter $\mathcal{R}$ is the radius of the outer template. $\mathcal{R} = 50$ in this study. Those pixels that are within 50 pixels to optic disc will have a d ranging from 50 pixels to 100 pixels, while those pixels that are within 50 pixels to fovea will get a d ranging from 0 pixels to 50 pixels. Since normally the distance between the optic disc and fovea in a fundus image is larger than 100 pixels, it is very unlikely for a pixel to fall in both side. Pixels that neither within $\mathcal{R}$ to optic disc or within $\mathcal{R}$ pixels to fovea will get a background value of 50 pixels. A true distance $\mathcal{D}$ map for Fig. 3.2 looks like Fig. 3.7.

www.manaraa.com

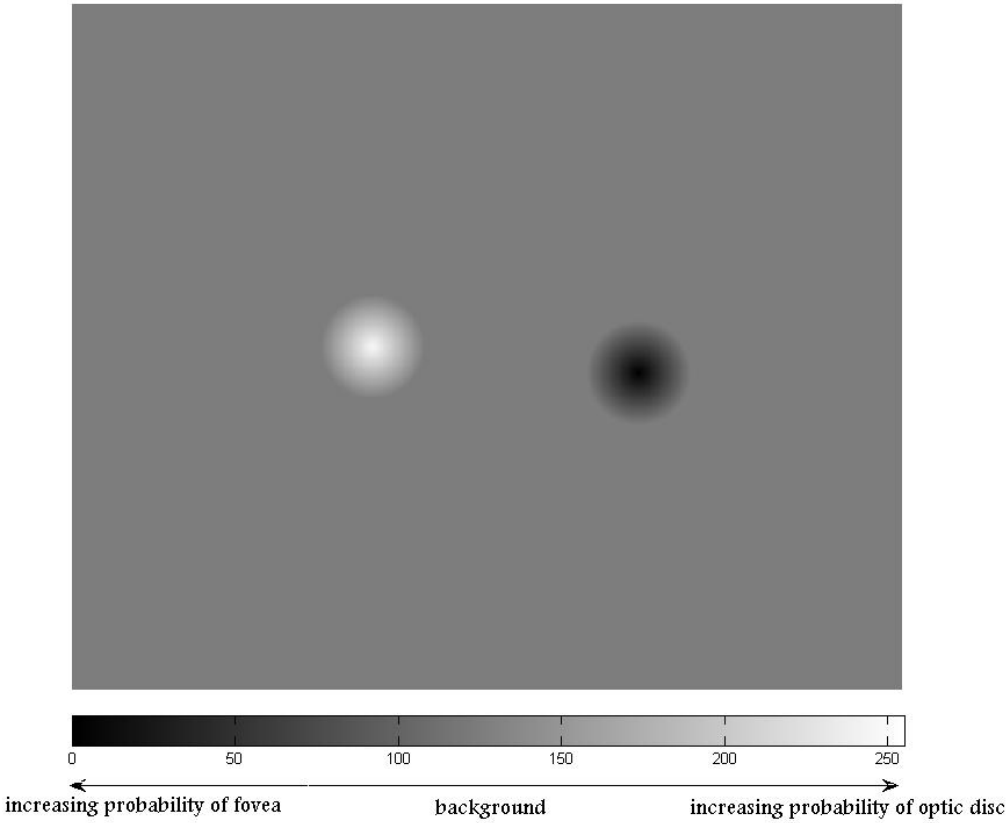

Figure 3.7: A standard true distance map for Fig 3.2(a). The background is normalized to 127. The higher the gray value is, the higher the probability of being within an optic disc. The lower the gray value is, the higher the probability of being within a fovea.

3.3 Feature Selection

After proposing all these potentially useful features, a feature selection method is necessary because all the features are not necessarily helpful. Also, the more features used, the slower the system tend to be. What we need is a compact set of features that can separate the optic disc and fovea from the background and the blood vessels to the largest extent.

A sequential forward and backward selection method is adapted [16]. This algorithm employs a $plus\, l, take\, away\, i$ strategy. Stating with an empty feature set,

www.manaraa.com

l features with the best combined performance are selected one by one and then i features are subtracted from the chosen feature group if by subtracting those features, the overall performance is better. This procedure goes on until the maximum feature number or a satisfactory performance is reached. The algorithm is given in Fig. 3.8.

In this study, the maximum feature number is set to 25. A larger number of feature will make the system very slow. The performance is measured as shown below.

Two criterion was proposed to measure the performance of the features. Criterion one is the rate of correctness. Criterion two is the mean distance.

$$\mathcal{C}1 = \begin{cases} \frac{N_{od|t}+N_{f|t}}{\mathcal{M}+\mathcal{N}} & \text{if} \quad \mathcal{M} > 3000, \mathcal{N} > 3000 \\ 0 & \text{otherwise} \end{cases} \tag{3.7}$$

Where $\mathcal{M}$ denotes the predicted number of pixels within $\mathcal{R}$ pixels to optic disc center and $\mathcal{N}$ denotes the predicted number of pixels within $\mathcal{R}$ ($R = 50$) pixels to fovea center. $N_{od|t}$ and $N_{f|t}$ denotes the number of pixels that are really within $\mathcal{R}$ pixels of the optic disc or fovea. $\mathcal{C}1$ ranges from 0 to 1. $\mathcal{C}1 = 1$ means that all the pixels detected as optic disc or fovea pixels are truly optic disc or fovea pixels. $\mathcal{C}1 = 0$ indicates that none of the pixels detected as optic disc/fovea pixels are really optic disc/fovea pixel.

$\mathcal{M} > 3000, \mathcal{N} > 3000$ guarantees that the detected pixels is not too small. 50 images are used to do the feature selection. So this condition guarantees that approximately 60 pixels are detected as optic disc and 60 pixels are detected as fovea on each test image. Without this limitation, solely the criterion is meaningless. For an extreme example, if only 1 points are detected from the 50 test images and it is

www.manaraa.com

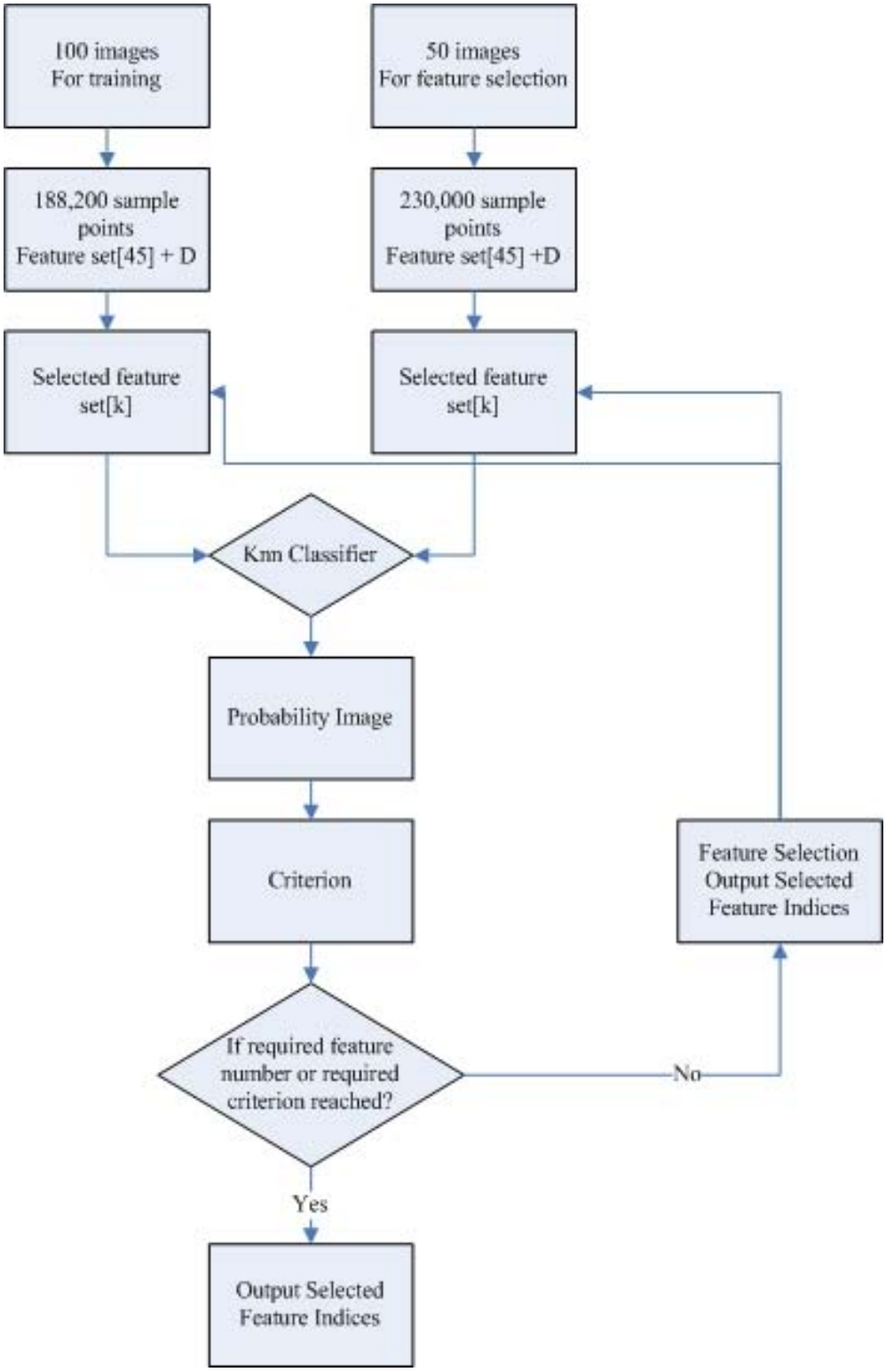

Figure 3.8: A flow chart to illustrate the feature selection procedure.

www.manaraa.com

within 50 pixels of the optic disc, then $\mathcal{C}1 = 1$, which might imply a very good result. But in fact it is not, because it lack the ability to detect any point from most of the images.

$$\mathcal{C}2 = \begin{cases} \frac{\sum_{i=1}^{\mathcal{M}} dist_{i|od} + \sum_{j=1}^{\mathcal{N}} dist_{j|f}}{\mathcal{M}+\mathcal{N}} & \text{if} \quad \mathcal{M} > 3000, \mathcal{N} > 3000 \\ 0 & \text{otherwise} \end{cases} \tag{3.8}$$

Similarly, $\mathcal{M}$ and $\mathcal{N}$ denotes the predicted number of pixels within R pixels within optic disc or fovea. $\sum_i^{\mathcal{M}} dist_{i|od}$ denotes the true distance to the optic disc for all $i \in \mathcal{M}$. $\sum_j^{\mathcal{N}} dist_{j|f}$ denotes the sum of true distance to the fovea for all $j \in \mathcal{N}$. $\mathcal{C}2$ ranges from 0 to $+\infty$. $\mathcal{C}2 = 0$ will imply that all $p \in \mathcal{M}$ are at the exact true location of the optic disc and all $p \in \mathcal{N}$ are at the exact true location of the fovea. The smaller the $\mathcal{C}2$ is, the better the performance.

The feature selection results using two different criterion are shown in Fig. 3.9. From the figures, we can see that, for both criterion, the performance fluctuates within a small range after five selected features. So even if the performance goes slightly better as more features are selected, the system becomes much slower. Also, too much features might cause over-fitting problems. So the first 11 selected features from both feature selections, which is a local maximum in $\mathcal{C}1$. The test results are shown in Fig. 3.10.

From the test images, we can see that $\mathcal{C}1$ performs lightly better than $\mathcal{C}2$. It deals with the images better at the edge of the images and it can better distinguish the optic disc from the large blood vessel. So, the first 14 features from $\mathcal{C}1$ are used for final test. They are listed in Table 3.2.

In the 14 selected features, two of them are from the green channel, but no feature from the red or blue channel is selected. This again proofs that the green

www.manaraa.com

Table 3.2: Selected features for the first k-NN classification.

feature #	feature description	template	image
1	number of vessels	quadrant 4	vessel image
2	average orientation difference	quadrant 3	vessel image
3	average orientation difference	quadrant 4	vessel image
4	standard deviation of orientation difference	quadrant 1	vessel image
5	standard deviation of orientation difference	quadrant 2	vessel image
6	standard deviation of orientation difference	quadrant 3	vessel image
7	standard deviation of orientation difference	quadrant 4	vessel image
8	orientation difference of max-width vessel	quadrant 3	vessel image
9	orientation difference of max-width vessel	quadrant 4	vessel image
10	vessel density	whole template	vessel image
11	standard deviation of image intensity	inner template	green channel image
12	standard deviation of image intensity	outer template	green channel image
13	average distance to nearest vessel pixel	inner template	distance image
14	max distance to nearest vessel pixel	inner template	distance image

www.manaraa.com

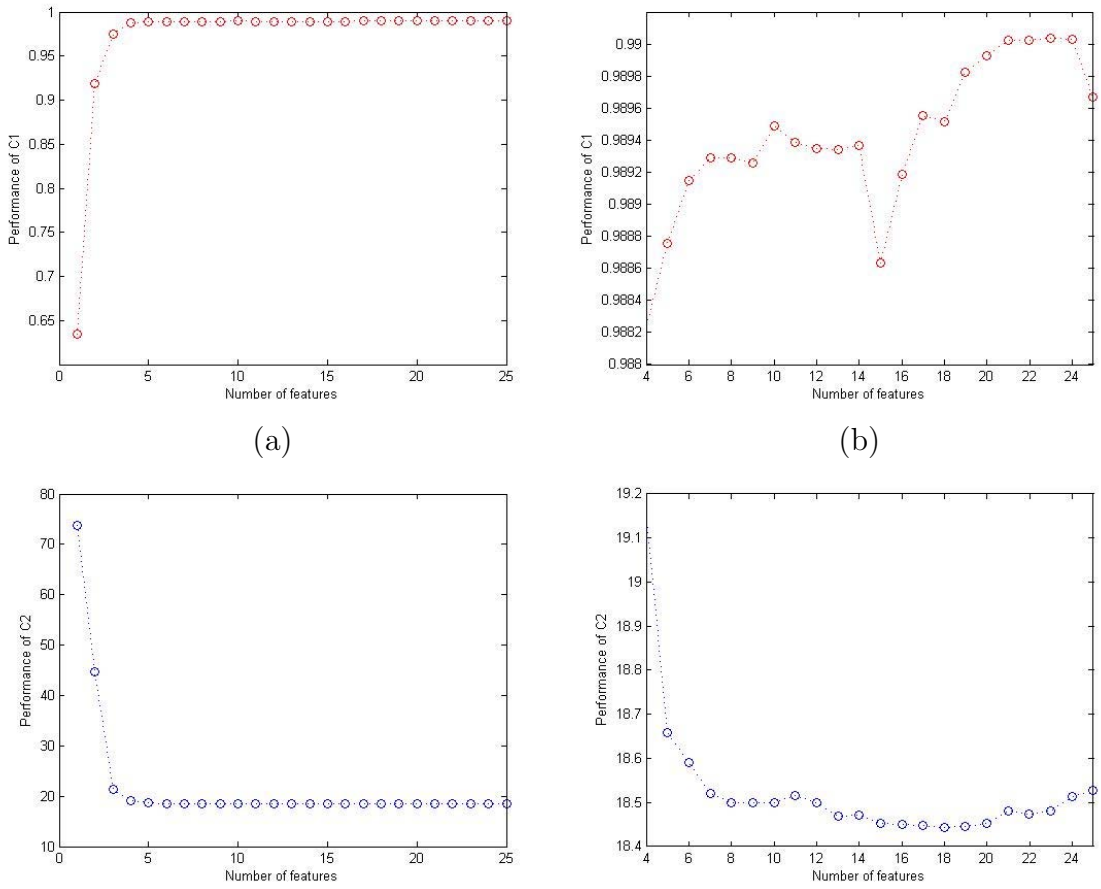

Figure 3.9: Feature selection with different criterions. (a)The performance of $\mathcal{C}1$ (1-25 selected features). (b)The performance of $\mathcal{C}1$ (4-25 selected features showing in details). (c)The performance of $\mathcal{C}2$ (1-25 selected features). (d)The performance of $\mathcal{C}2$ (4-25 selected features showing in details).

channel contains more information than the red channel and blue channel.

3.4 First *k*-NN Classification

During the training phase, the relationship is build between the selected feature and the dependent variable $\mathcal{D}$. For each training image, a rectangular grid of size $(2\mathcal{R})^2$ is centered at the optic disc and fovea separately. Inside the rectangular grid, the image is sampled densely for every 5 pixels, Then a number of 1000 sample points are randomly picked within the whole image. So a total number of 188,200 sample

www.manaraa.com

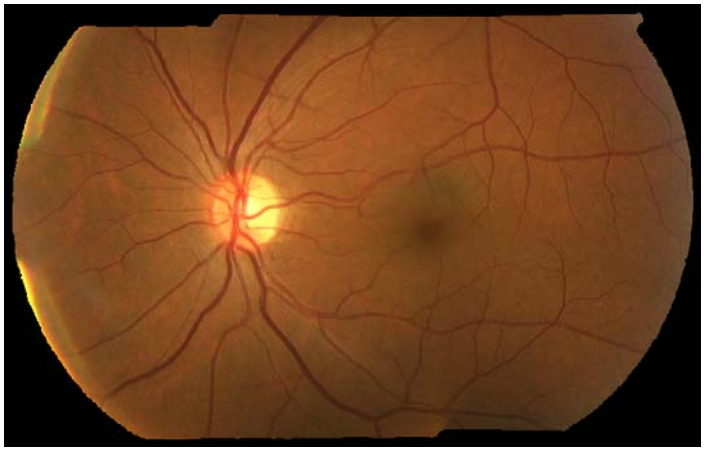

(a)

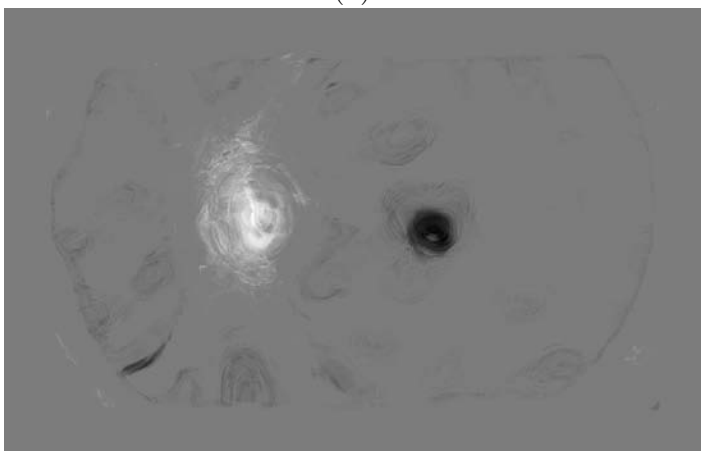

(b)

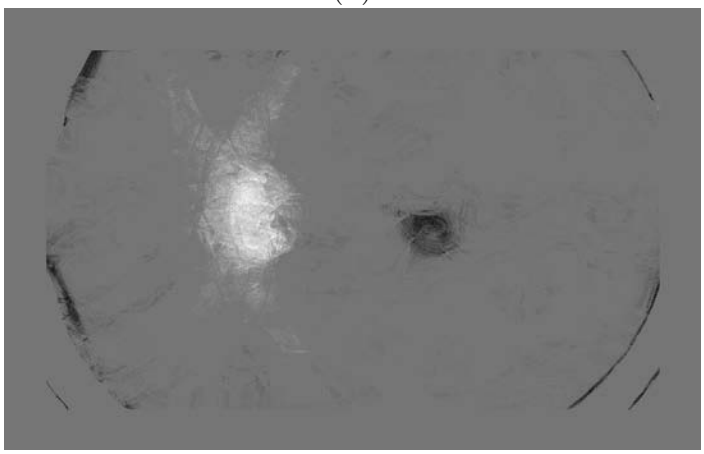

(c)

Figure 3.10: Criterion comparison. (a)Fundus image. (b)Result image using first 11 selected features from $\mathcal{C}1$. (b)Result image using first 11 selected features from $\mathcal{C}2$. $\mathcal{C}1$ performs better than $\mathcal{C}2$ at the image FOV boundary. For images (b) and (c), the background is normalized to 127. The higher the gray value is, the higher the probability of being within an optic disc. The lower the gray value is, the higher the probability of being within a fovea.

www.manaraa.com

points are used to train the system. The circular template is placed on every sample point. The features are measured around the template and the dependent variable d is calculated.

During test, the same set of features is measured for every pixel in the image. To estimate the distance d, the k nearest neighbors in the feature space are found and the values d of these nearest neighbors are averaged. k is chosen to be 11 in this study.

An simple illustration of how k-NN works is shown in Fig. 3.11. In this simple example, the red circles denote optic disc pixels ($\mathcal{D} > 50$). The blue stars denote fovea pixels ($\mathcal{D} < 50$).The black triangles denotes background pixels ($\mathcal{D} = 50$). Green star is the test pixel. $k = 5$ is used. Three red circles, one blue star and one black triangle are found as the five nearest neighbors for the testing green star. Suppose the $\mathcal{D}$ associated with the the five neighbors are 75, 70, 65, 50, 45 respectively. We can calculate the $\mathcal{D}$ associated with the testing green star to be $\frac{75+70+65+50+45}{5} = 61$.

After the first k-NN classification, a soft label is assigned to every pixel in the image. A value larger than 50 indicates that this pixel is likely to be an optic disc pixel. The larger the value, the higher the likelihood is. Similarly, a value smaller than 50 indicates a possibility of being a fovea center, the lower the pixel value, the larger the probability.

If the original fundus image is of high image quality, and no severe disease presented, the result from the first k-NN classification is good enough to give a valid estimation of the optic disc and fovea location. A result image is shown is Fig. 3.12.

www.manaraa.com

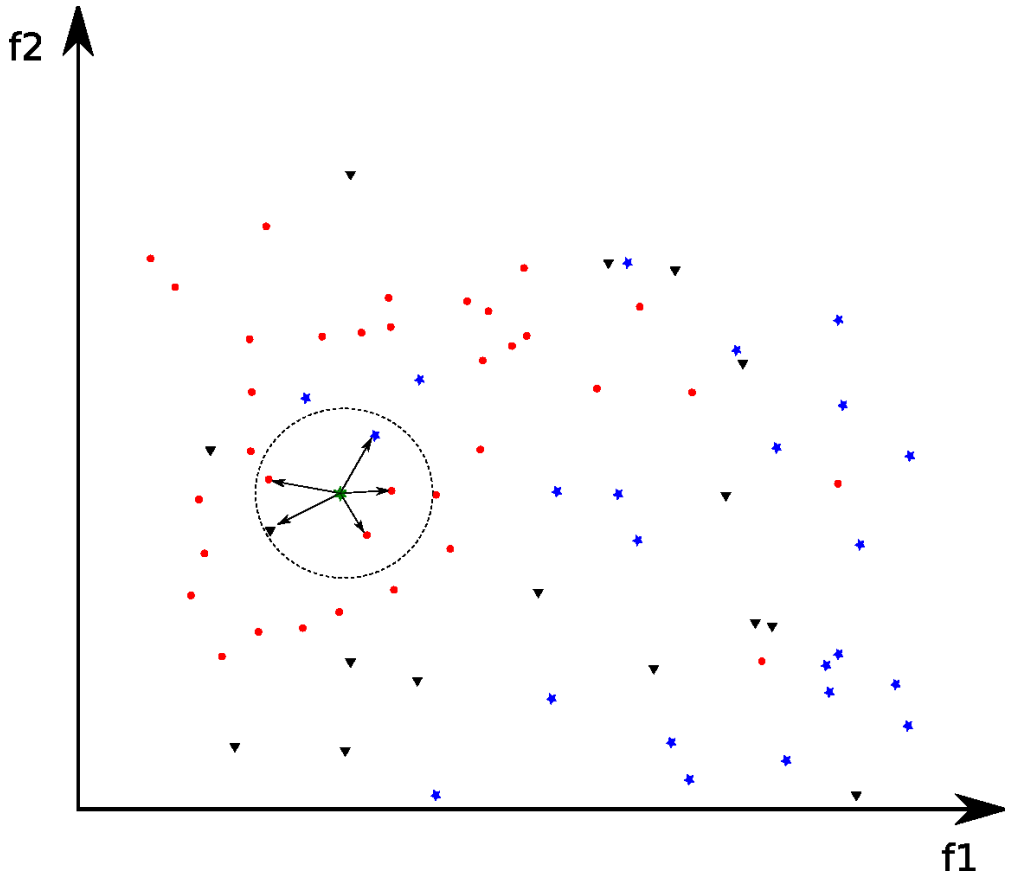

Figure 3.11: An illustration of k-NN regression. k=5 neighbors are found in this example. The red circles denote optic disc pixels ($\mathcal{D} > 50$). The blue stars denote fovea pixels ($\mathcal{D} < 50$). The black triangles denotes background pixels ($\mathcal{D} = 50$). Green star is the test pixel.

3.5 Second k-NN Classification

A first k-NN classification can give a good detection result for most cases. But when diseases appears or image quality is low, detection failures might occur. Within the detection failure cases, most of them have one structure, either optic disc or fovea, detection failed. The reason is usually that, there is some other areas has a higher probability than the true location does.

A second k-NN regression is applied to further enhance the result. During the first k-NN regression, the same set of features are applied to distinguish the optic disc

www.manaraa.com

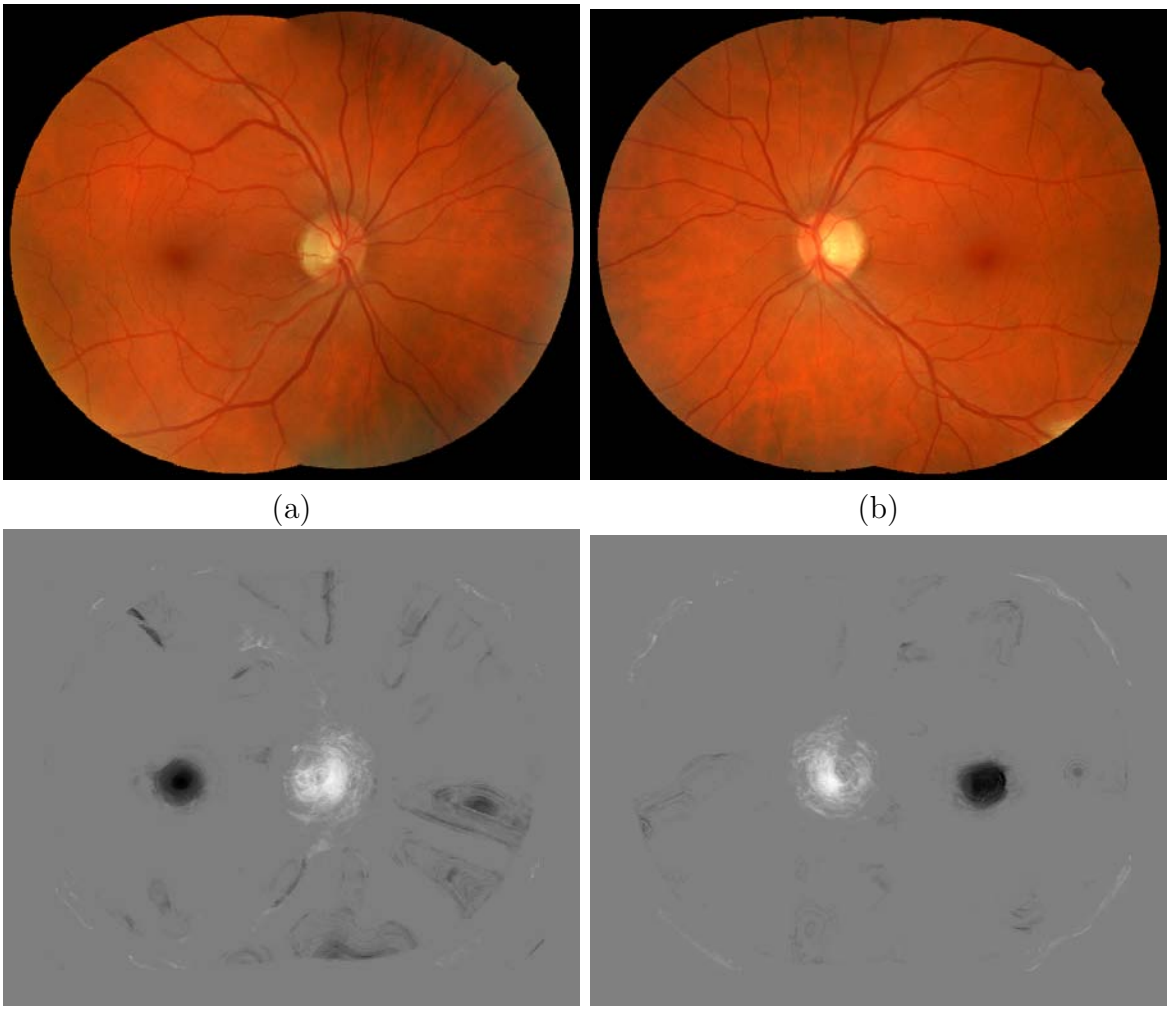

Figure 3.12: Results of first k-NN classification. (a),(b): The fundus images of the left eye and right eye from the same person. (c),(d):Result image from the first k-NN classification. The background is normalized to 127. The higher the gray value is, the higher the probability of being within an optic disc. The lower the gray value is, the higher the probability of being within a fovea.

www.manaraa.com

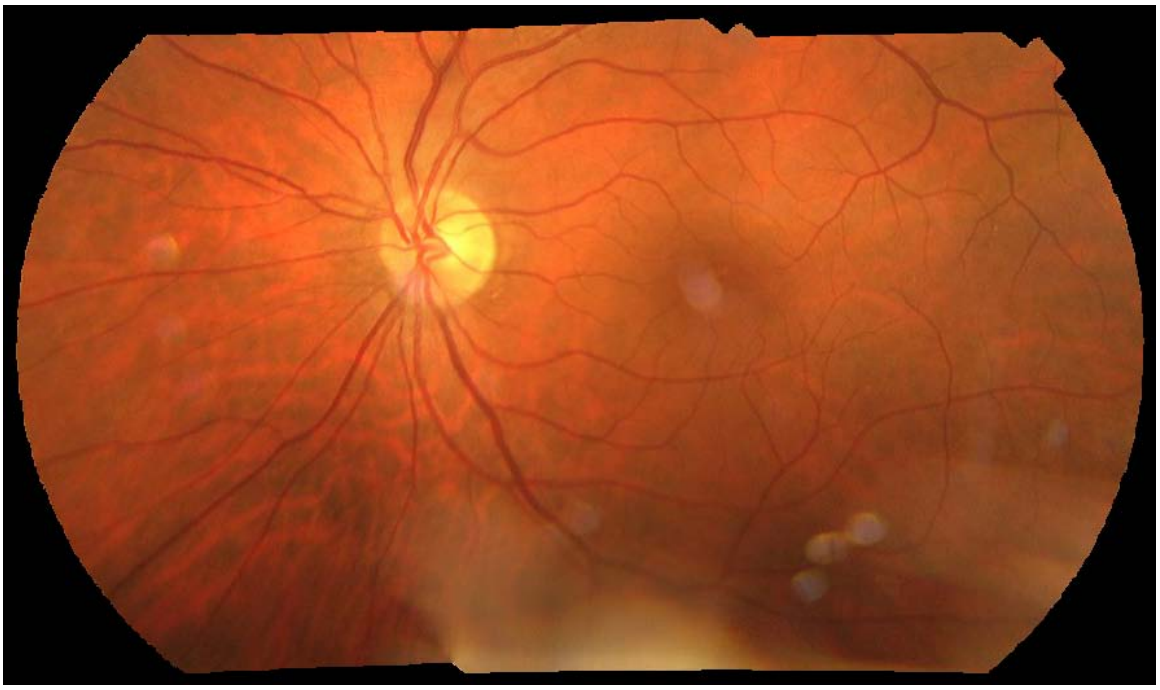

(a)

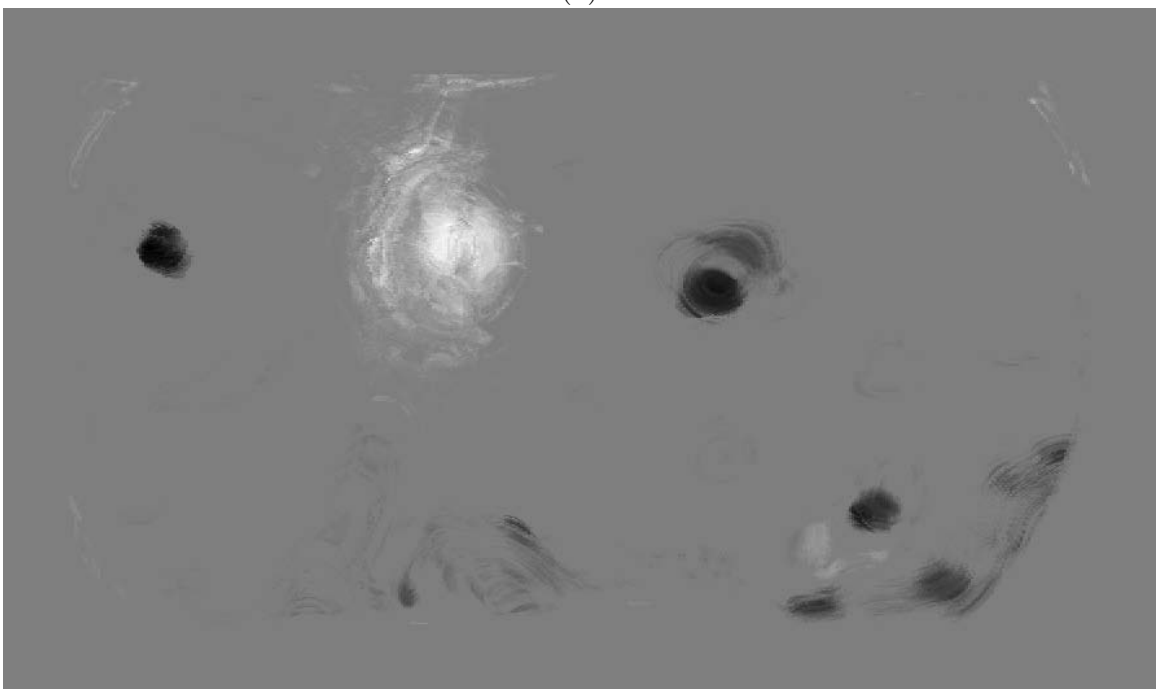

(b)

Figure 3.13: A example of first k-NN classification result. Two large regions on the image are labeled as fovea. The region on the left is falsely detected. (The background is normalized to 127. The higher the gray value is, the higher the probability of being within an optic disc. The lower the gray value is, the higher the probability of being within a fovea.)

www.manaraa.com

Table 3.3: Features extracted for the second k-NN classification

for optic disc pixels	for fovea pixels
pixel intensity	pixel intensity
distance to fovea center	distance to optic disc
angle to fovea center	angle to optic disc

and fovea from the other structures simultaneously. But no mutual information is included. Actually, in a fundus image, the distance between the optic disc and fovea as while as the angle between them has some potential patterns and might be used to enhance the detection result.

During training, for every pixel that is assigned as an optic disc/fovea pixel in the first stage, three more features are extracted from the probability image and a similar dependent variable d with is assigned to it.

During test, first the whole probability map is scanned and the maximum value and minimum value is stored as detected optic disc and fovea. Then same features as in training are extracted and a set of $k = 11$ nearest neighbors in the feature space are found. The corresponding d are averaged and assigned as a second probability label.

Examples of the second k-NN regression is shown in Fig. 3.14 and Fig. 3.15. For Fig. 3.14, image (a) is a fundus image. Image (b) is the first k-NN result of (a). The optic disc and fovea are detected correctly. (c) is the second k-NN regression of (a). Because the detection result of first k-NN is both correct, the optic disc and fovea locations are both enhanced, for they satisfy a relative location relationship as trained. For Fig. 3.15, image (a) is a fundus image. Image (b) is the first k-NN regression of (a). The optic disc is detected correctly, while the fovea is detected at

www.manaraa.com

the bottom dark region (circled in red). Image (c) is the second k-NN regression result of (a). Because the optic disc is detected correctly, it is able to enhance the true fovea location. All other dark regions are suppressed, as shown on (d). But the incorrect fovea detection result is unable to enhance any region on the image, because no bright region is on the expected location.

The essential idea is that, since the features are based on distances and angles between optic disc and fovea, it is actually a mutual enhancement procedure. Given one detected structure location, the other structure will be expected to be in a certain location with the first structure. If there happened to have pixels labeled as the second structure, it will be enhanced. But if there is no such pixels or the likelihood is very weak, meaning the gray value is near 50, those pixels will not get enhanced.

When the second k-NN regression is finished, it is combined with the first k-NN regression. For the pixels detected to be optic disc pixels, the probability is added to the first probability map to make the gray value even higher. While for those pixels detected to be fovea pixels, the gray value is subtracted from the first probability image to make the gray value even lower. The reason why not solely use the second probability map is that, as shown in Fig. 3.14 and Fig. 3.15, if there is one falsely detected structure, it will not be able to enhance the other structure. Hence there might have only one enhanced structure on the second probability map.

3.6 Image Post-processing

To find the optic disc and fovea, the final probability image is blurred, with a Gaussian kernel with $\sigma = 15$. This value is empirically determined. It dose not have a big influence on the final result. Finally, the pixel with the highest value is selected

www.manaraa.com

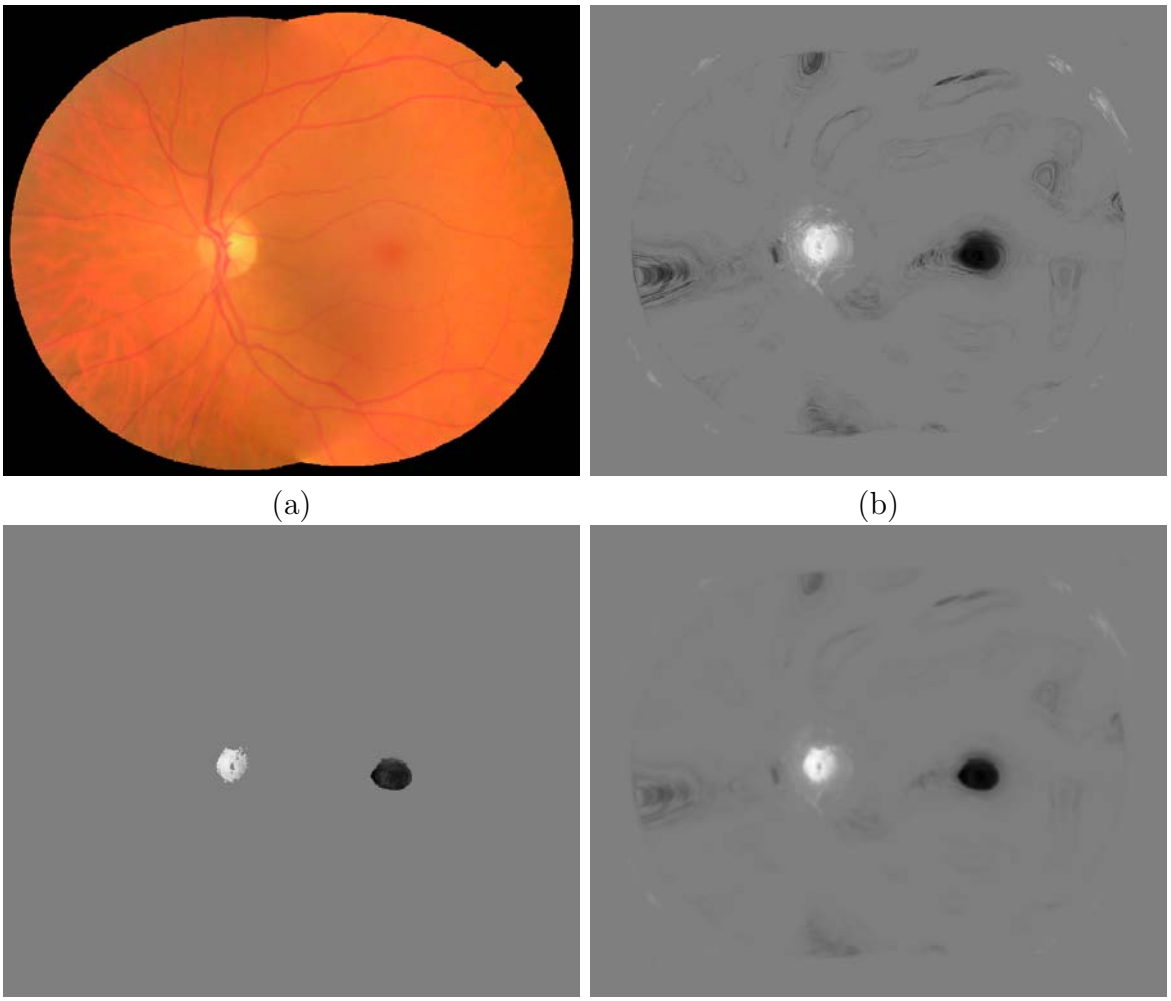

(a) (b)

(c) (d)

Figure 3.14: An example to illustrate the impact of second k-NN classification on the result image. (a)Fundus image. (b)The probability image resulting from the first k-NN classification. Both optic disc and fovea are detected correctly. (c)The probability image resulting from the second k-NN classification. Both optic disc and fovea get enhanced. (d)Final result image. False probability regions are suppressed. (The background is normalized to 127. The higher the gray value is, the higher the probability of being within an optic disc. The lower the gray value is, the higher the probability of being within a fovea.)

www.manaraa.com

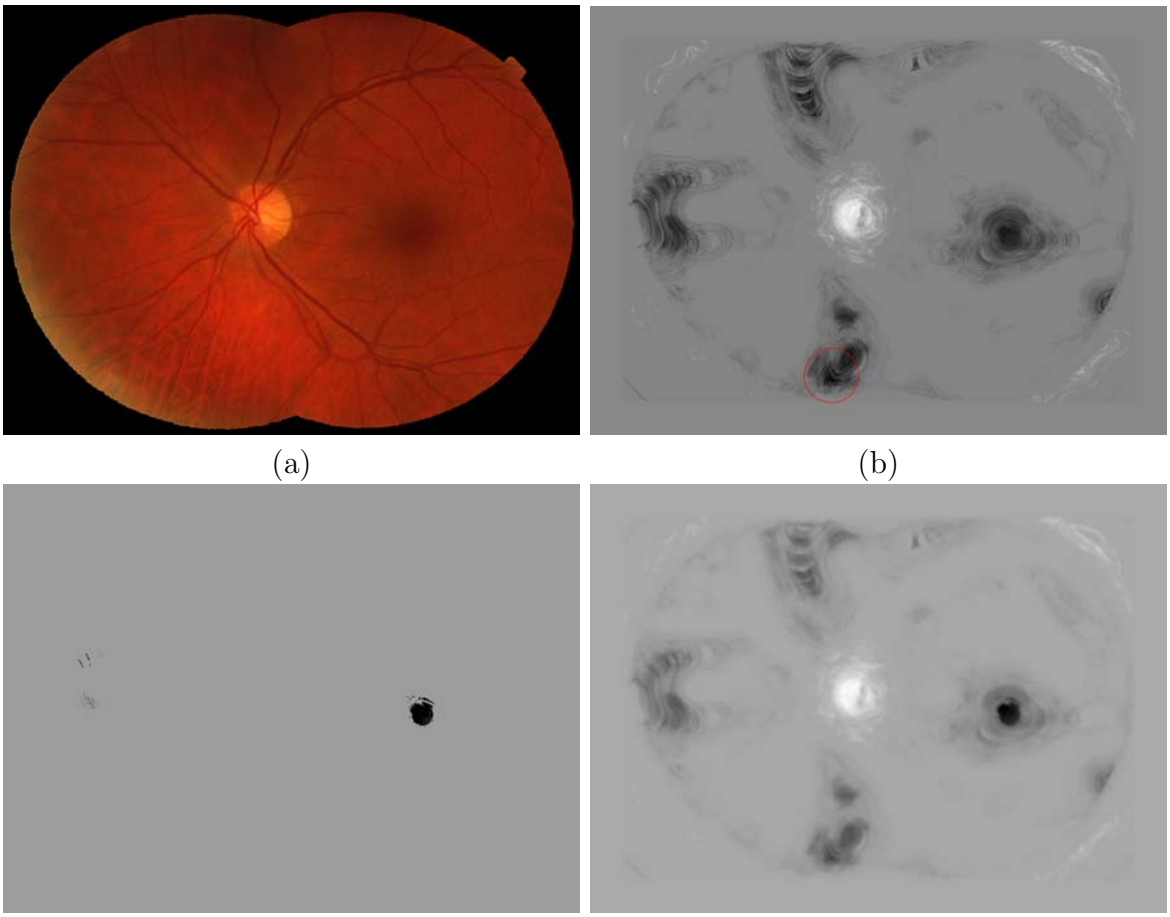

(a) (b)

(c) (d)

Figure 3.15: A second example to illustrate the impact of second k-NN classification on the result image. (a)Fundus image. (b)The probability image resulting from the first k-NN classification. The fovea detection is incorrect. (c)The probability image resulting from the second k-NN classification. The enhanced fovea appears on the image. (The optic disc does not get enhanced because it does not get support from the detected fovea location on the first k-NN classification.) (d)Final result image. False probability regions are suppressed.

www.manaraa.com

as the optic disc location and the pixel with the lowest value is selected as the fovea location.

www.manaraa.com

CHAPTER 4
EXPERIMENTAL METHODS

4.1 Data

Two hundreds normal fundus images of the let eye were used to train the system. One hundred and fifty of them were used for first k-NN training. Fifty images were used for feature selection. Fifty images were used for the second k-NN training.

A set of 479 fundus images with early diabetic retinopathy were used to test the system. Two hundreds and forty of them are left eye images. Two hundreds and thirty nine of them are right eye images. The right eye images were manually identified and flipped before the test and the output images were flopped back.

4.2 Training Phase

During the first k-NN training and feature selection, the relationship between a set of features and the dependent variable $\mathcal{D}$ is built. For each training image, a rectangular grid of size $(2\mathcal{R})^2$ is centered at the optic disc and fovea separately. Inside the rectangular grid, the image is sampled densely for every 5 pixels, which is 882 sample points for both rectangular grids. Additionally, a number of 1,000 sample points are randomly picked within the whole image. In total, 1882 locations are sampled on each image, which is 188,200 sample points for the whole 100 training set.

For each sample point, the circular template is placed on it. The features are measured within the template and dependent variable $\mathcal{D}$ is calculated.

www.manaraa.com

Image sampling during second k-NN regression is a little different. Instead of a densely sample plus random sample, the first probability image is thresholded at 170 and 80 separately. All pixels that have a gray value larger than 170 on the first probability image are picked for otic disc training. Similarly, all pixels that have a gray value smaller than 80 on the first probability image are picked for fovea training.

4.3 Test Phase

During test, in order to save running time, not every pixel on the image is measured. Intuitively a down-sample, up-sample method may be more preferable. But image down sample will change some features, of the image, such as vessel width, and vessel number. So features are only calculated for even column pixels. The odd column will get a probability value through nearest neighbor interpolation.

Pixels within $\mathcal{D}$ pixels to the image boundary are not considered and labeled as background.

www.manaraa.com

CHAPTER 5
RESULTS

5.1 Result for Certain Features

Some of the feature images are listed in Fig. 5.1. Because the template size is $\mathcal{R}$ ($\mathcal{R} = 50$) pixels, the pixels with a distance smaller than $\mathcal{R}$ pixels to the image boundary is not calculated. Fig 5.1 (c) shows the average intensity of the inner template. It is very reasonable that the vessel density is higher at the optic disc area and lower at the fovea area. The left FOV boundary has a high gray value also because of a high intensity around that area on the fundus image. Figure 5.1 (d) is the average vessel width over the whole template. The places where the large vessels locate have a relatively higher gray value. In the fovea area where fewer blood vessels present, the gray value is reasonably lower. Figure 5.1 (e) is the vessel density for the whole template. As expected, the locations where vessel density are high have larger gray values. The fovea area and the four corners, where fewer vessels present, have lower gray values. At last, Fig. 5.1 (f) shows the maximum distance to the nearest vessel in the inner template. So the gray value distribution on this image is very different with (d) and (e). In the neighboring area of the blood vessel, the maximum distance to a blood vessel is small, resulting in a low gray value. However, in the places absence of blood vessels, pixels have a higher gray value for they have higher distance to a blood vessel.

www.manaraa.com

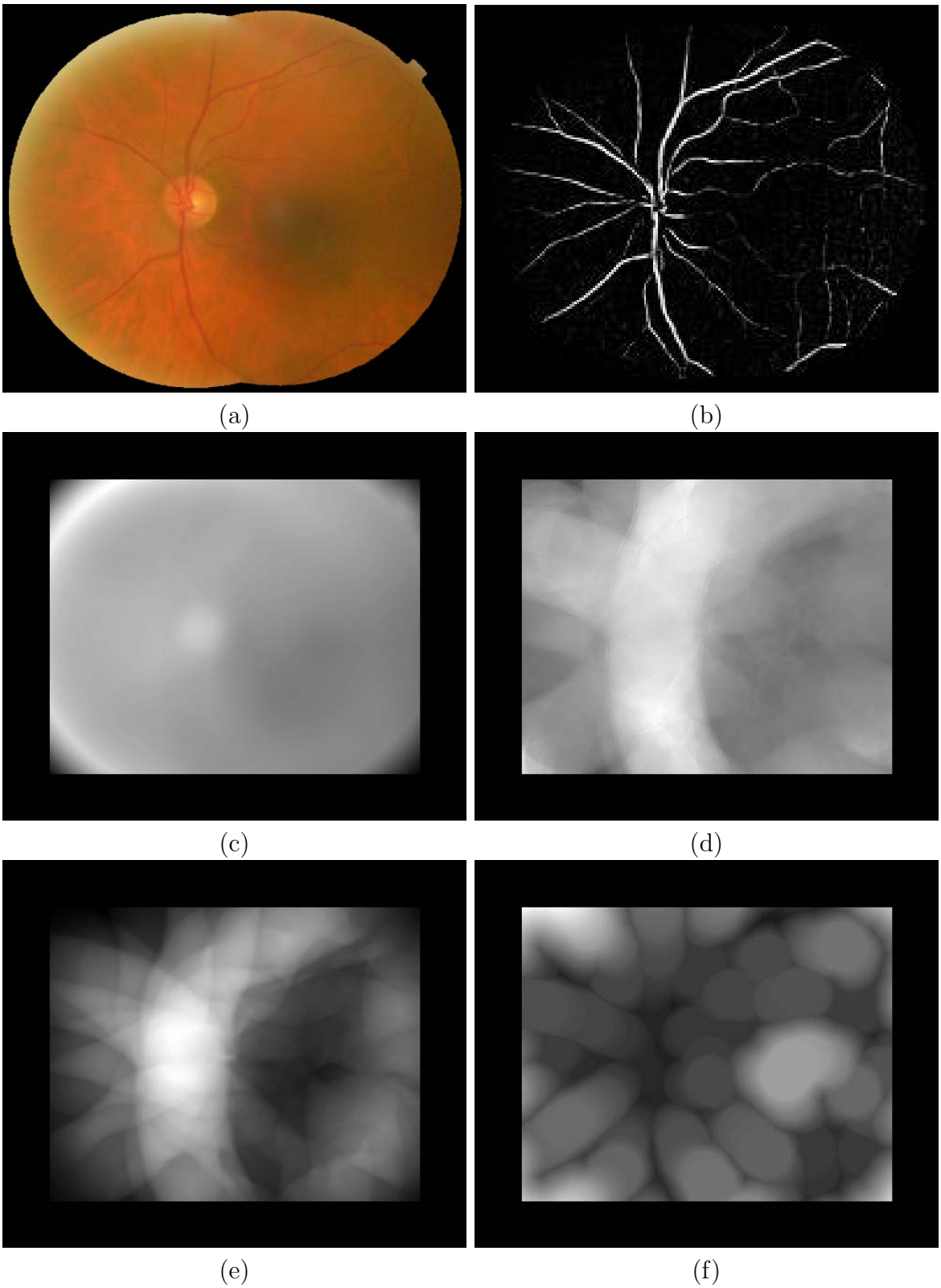

Figure 5.1: Feature images. Higher gray value indicates a higher response of the specified feature kernel. (a)One fundus image. (b)The vessel probability image of (a). (c)The average intensity of the inner template. (d)The average vessel width over the whole template. (e)Vessel density for the whole template. (f)The maximum distance to the nearest vessel in the inner template.

www.manaraa.com

5.2 First k-NN Classification Results

Typical result images from the first k-NN classification is shown in Fig 5.2. The high gray value regions indicate the possible locations of the optic disc, while the low gray value regions indicate the possible locations of the fovea. The background is normalized to gray level 127.

Some good results will have only have one bright region and one dark region, like in case (a), (c), (d) (g) and (h). In these cases, the estimated locations will be accurate and clear. On the other hand, other cases might get more than one bright regions or dark regions, like in case (b), (e) and (f). Possible reasons include the presence of disease, low image contrast, artifacts or unbalanced illumination. Among those cases, it is possible to finally detect correct locations. However, this is not guaranteed. In some really bad cases as shown in (b), it is very hard to tell where is the estimated fovea.

In order to solve this problem, the second k-NN classification is introduced. The results are analyzed in Section 5.3.

5.3 Second k-NN Classification Results

The corresponding second k-NN results for images in Fig. 5.2 is shown in Fig. 5.3.

As described in Section 3.5, the second k-NN classification includes certain mutual information between the optic disc and the fovea and thus it is able to only enhance the bright/dark regions that get support from the dark/bright regions. Hence the cases shown in Fig. 5.2 (b), (e) and (f) can be handled very nicely (as shown in Fig. 5.3 (b), (e) and (f)). The misleading dark regions get suppressed.

www.manaraa.com

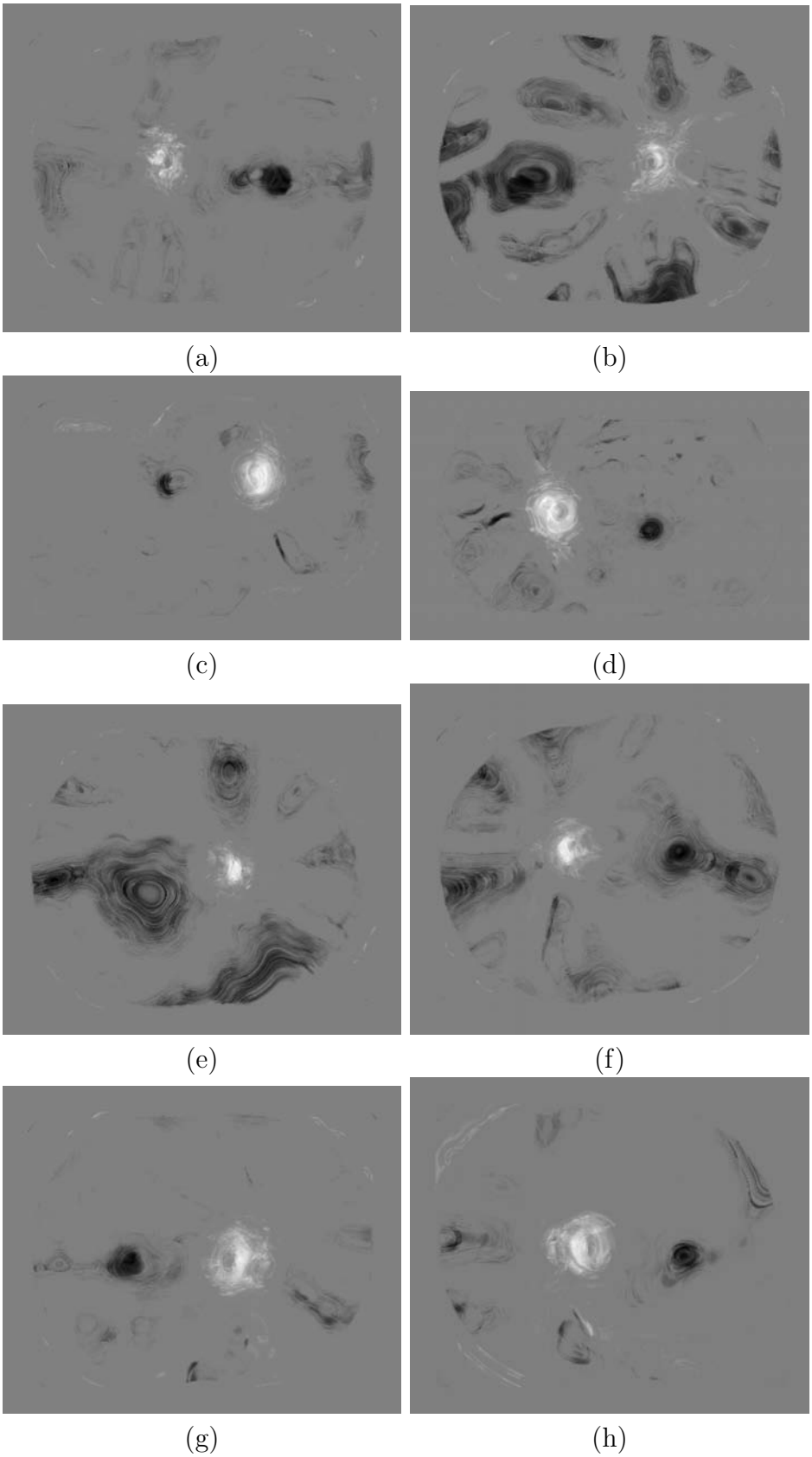

Figure 5.2: Examples of typical result of first k-NN classification. Each row shows a paired left eye and right eye result from the same person. The background is normalized to 127. The higher the gray value is, the higher the probability of being within an optic disc. The lower the gray value is, the higher the probability of being within a fovea.

www.manaraa.com

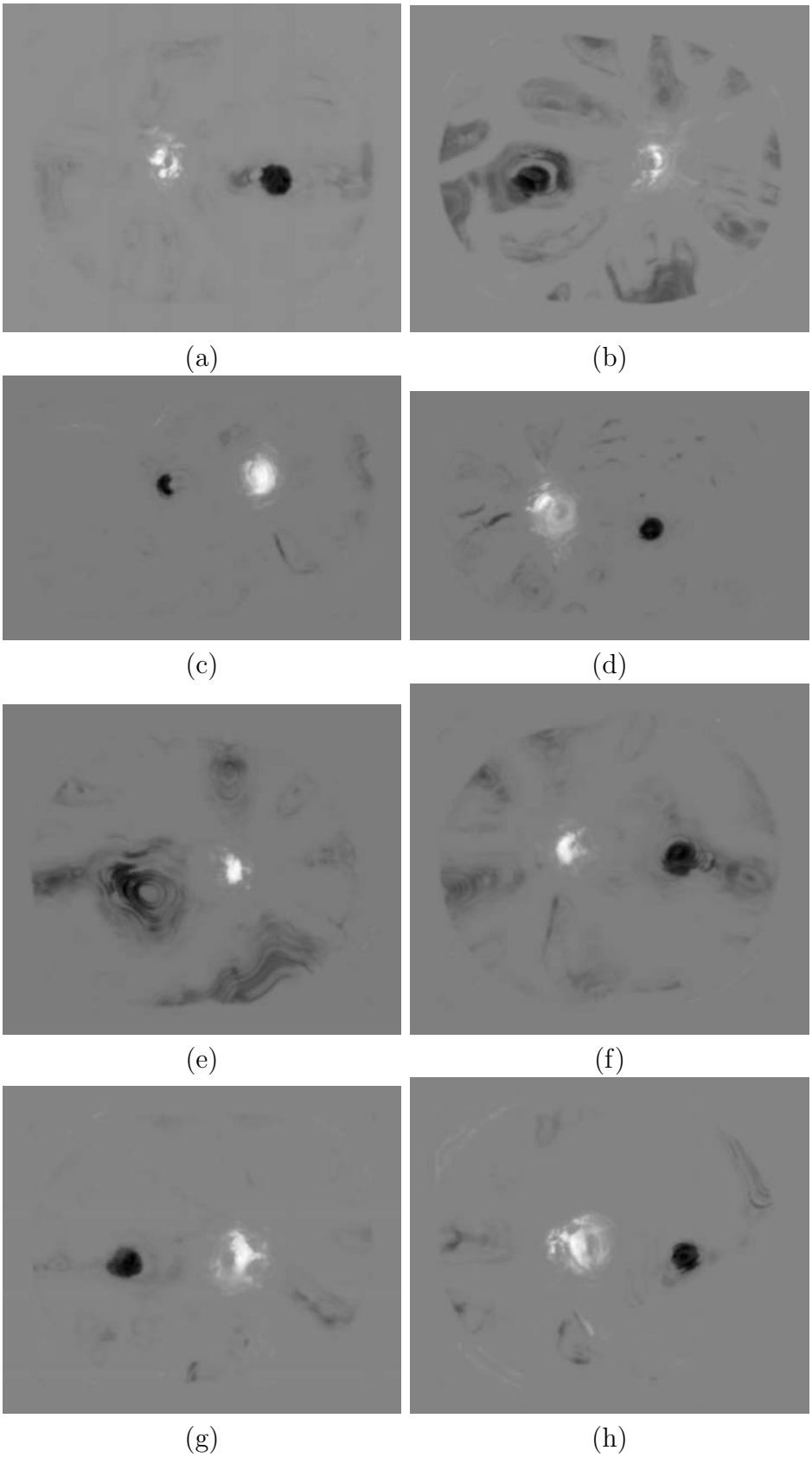

Figure 5.3: Examples of typical result of second k-NN classification. Each row shows a paired left eye and right eye result from the same person. The false responses has been suppressed. The higher the gray value is, the higher the probability of being within an optic disc. The lower the gray value is, the higher the probability of being within a fovea.

www.manaraa.com

Table 5.1: Overview of test results

	left eye		right eye	
number of images	103		207	
	optic disc	fovea	optic disc	fovea
mean of distance error	19.6640	34.5459	20.6351	31. 1866
standard deviation of distance error	31.9516	63.9703	36.7664	51.1050
correct rate	93.2%	88.4%	94.0%	87.9%

5.4 Statistical Results

The test database is constitutive of 103 left eye images and 207 right eye images with early sign of diabetic retinopathy. The general statistic results are shown in Table 5.4.

5.4.1 General Analysis

For all the 310 images, the mean distance error is 20.31 pixels with a standard deviation of 35.19 pixels for the optic disc. 98.1% estimated results fall in a circle with a radius of $\mathcal{R} = 100$ centered at the true location. 93.9% estimated results fall in a circle with a radius of $\mathcal{R} = 50$ pixel centered at the true location (as shown in Fig. 5.5).

For the fovea, the mean distance error is 32.31 pixels with a standard deviation of 55.62 pixels. 95.8% estimated results fall in a circle with a radius of $\mathcal{R} = 100$ centered at the true location. 88.1% estimated results fall in a circle with a radius of $\mathcal{R} = 50$ pixel centered at the true location.

The histograms of the distance error is shown in Fig. 5.4.

The correlated distance error is shown in Fig. 5.5. Most of the points are located both within 50 pixels to the true location of the optic disc and 50 pixels to the true location of the fovea. The distance error for the fovea is slightly more

www.manaraa.com

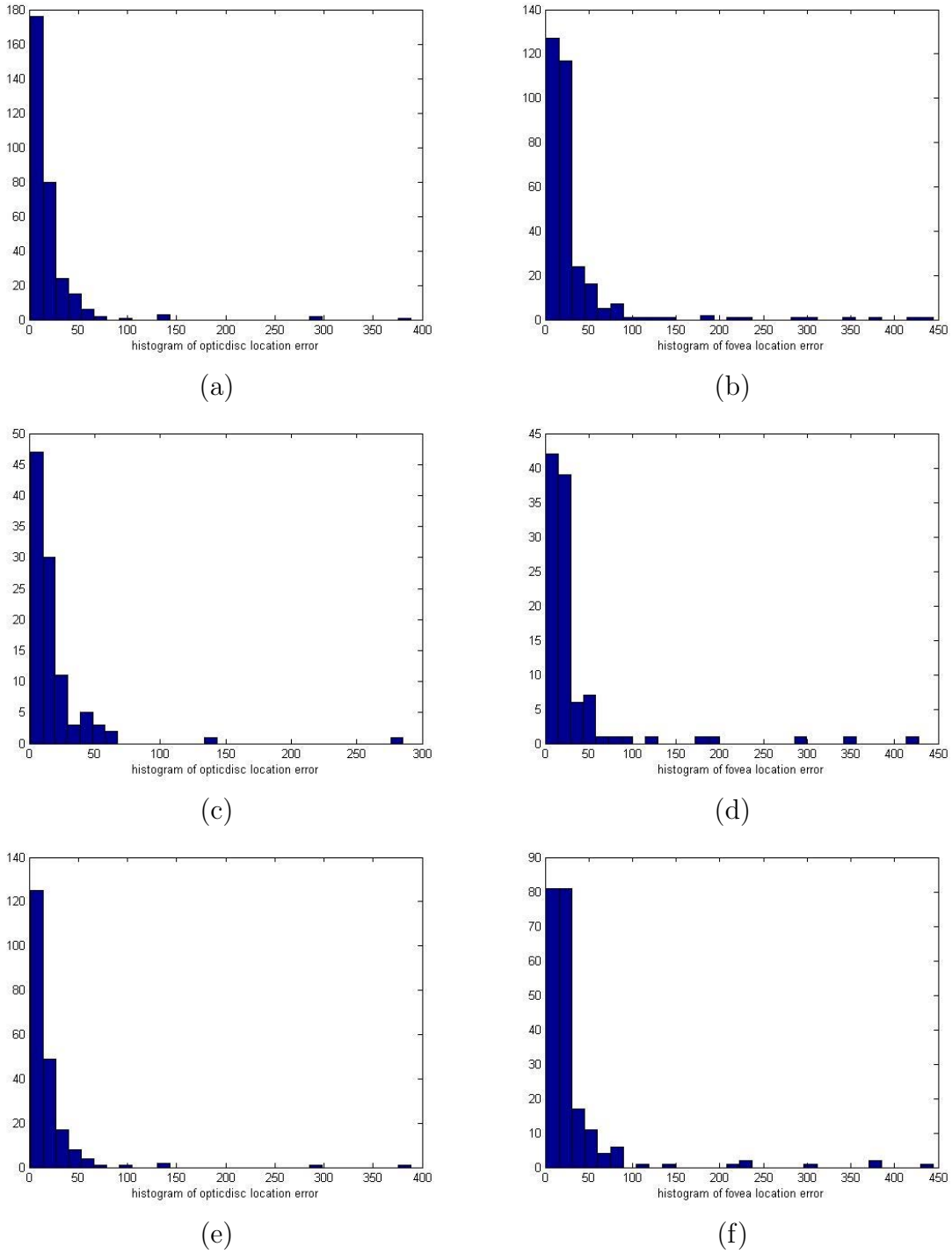

Figure 5.4: Histograms. Images (a),(b) are the general distance errors of the optic disc and fovea. Images (c),(d) are the distance errors of the left eye. (e), (f) are the distance errors of the right eye.

www.manaraa.com

dispersive than the optic disc. Most images only have one estimation error (if there is any), except for three outliers.

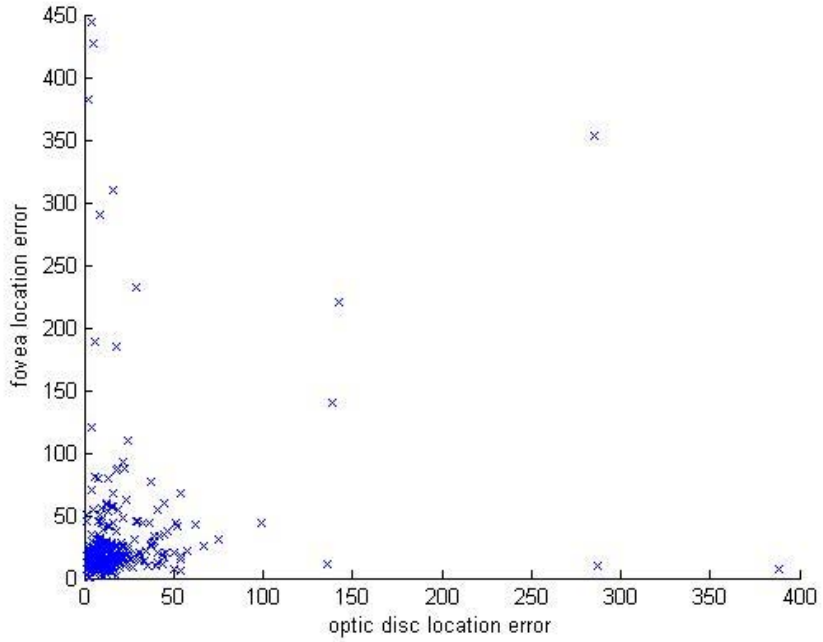

Figure 5.5: The correlated error of the optic disc and fovea for both eye images. The x-axis is the distance error of the optic disc. The y-axis is the corresponding distance error of the fovea.

5.4.2 Left Eye Analysis

For the left eye images, the mean distance error and standard deviation of the optic disc is 19.66 pixels and 31.95 pixels. 98.1% estimated results fall in a circle with a radius of $\mathcal{R} = 100$ centered at the true location. 93.2% estimated results fall in a circle with a radius of $\mathcal{R} = 50$ centered at the true location.

The mean distance error and standard deviation of the fovea for the left eye is 34.54 pixels and 63.97 pixels, which is a little higher than the optic disc. 94.2% estimated results fall in a circle with a radius of $\mathcal{R} = 100$ centered at the true location.

www.manaraa.com

88.4% estimated results fall in a circle with a radius of $\mathcal{R} = 50$ centered at the true location.

The histogram of the distance error for the left eye is shown in Fig. 5.4.

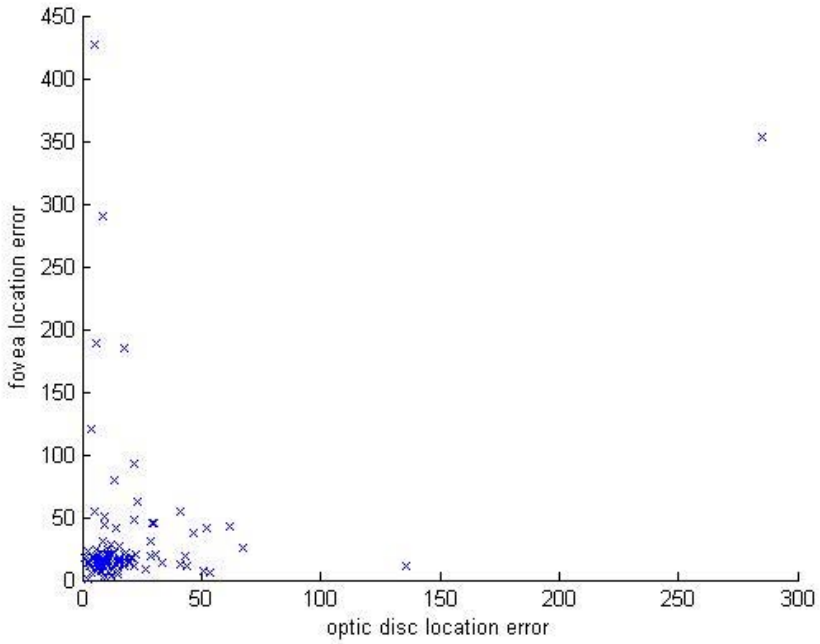

Figure 5.6: The correlated error of the optic disc and fovea for the left eye images. The x-axis is the distance error of the optic disc. The y-axis is the corresponding distance error of the fovea.

The correlated error is shown in Fig. 5.6. The figure shows the distance error of the optic disc and fovea of the same image together. There is one outlier on the top right corner, which means the distance error of the optic disc and fovea are both very high. Other than that, most of the images have a correlated distance error within the 50 pixel-50 pixel rectangular. We can also see that the fovea detection is a little bit worse than the optic disc detection.

Fig. 5.7 shows all the detected location on one image. The true locations of

www.manaraa.com

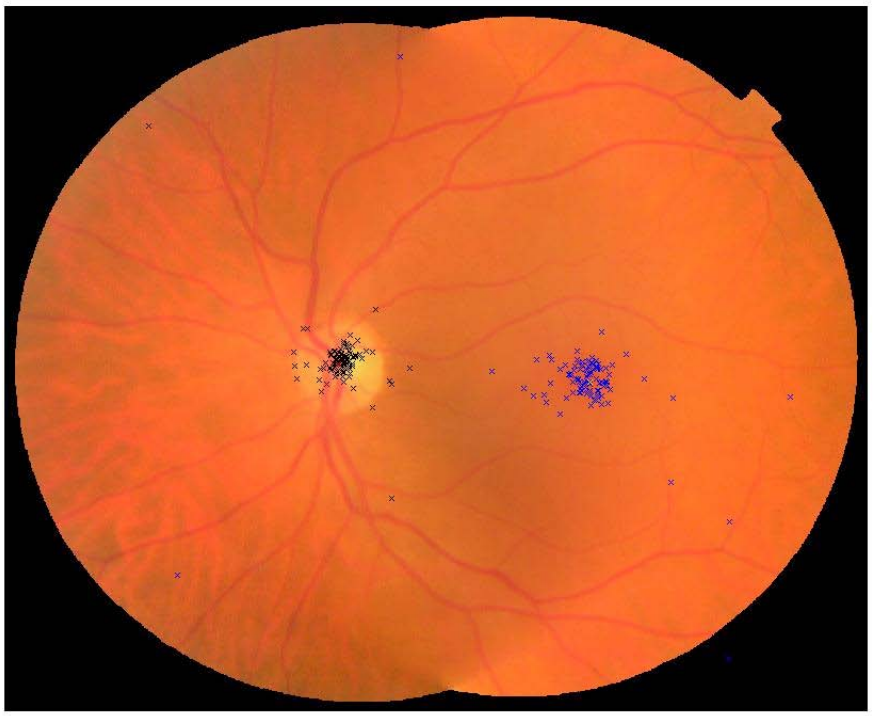

(a)

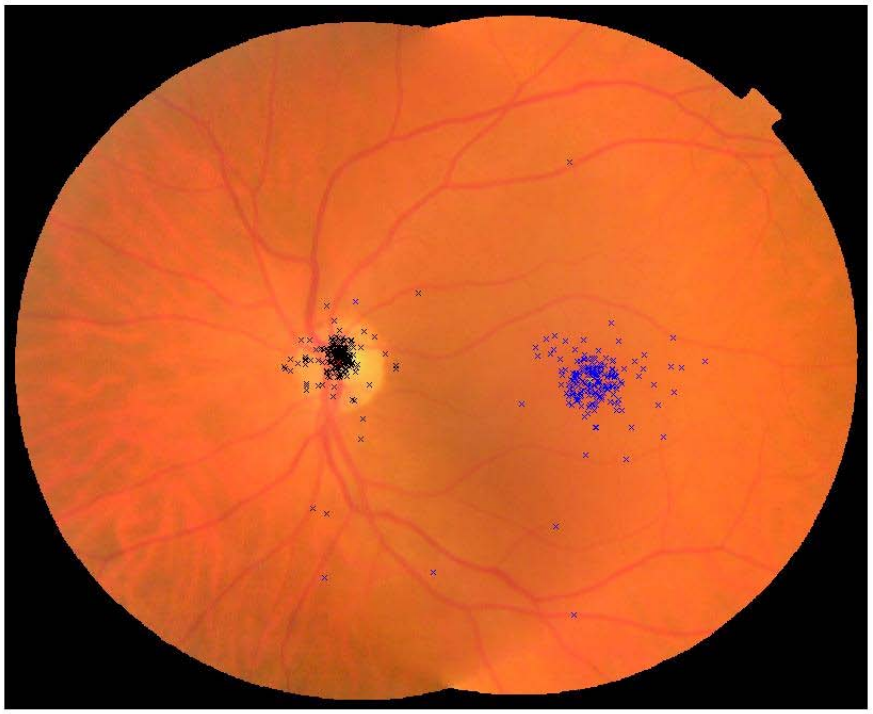

(b)

Figure 5.7: Scatter plots of all detected location on one fundus image. The true locations have been normalized to the true location of the shown fundus image. (a)Scatter plot of the left eye. (b)Scatter plot of the right eye.

www.manaraa.com

the optic discs have been registered to the true location of the optic disc of this given image. The true locations of the foveae have been registered to the true location of the fovea of this given image as well.

5.4.3 Right Eye Analysis

For the 207 right eye images, the mean distance error and standard deviation of the optic disc are 20.63 pixels and 36.76 pixels. 98.1% estimated results fall in a circle with a radius of $\mathcal{R} = 100$ centered at the true location. 94.2% estimated results fall in a circle with a radius of $\mathcal{R} = 50$ centered at the true location.

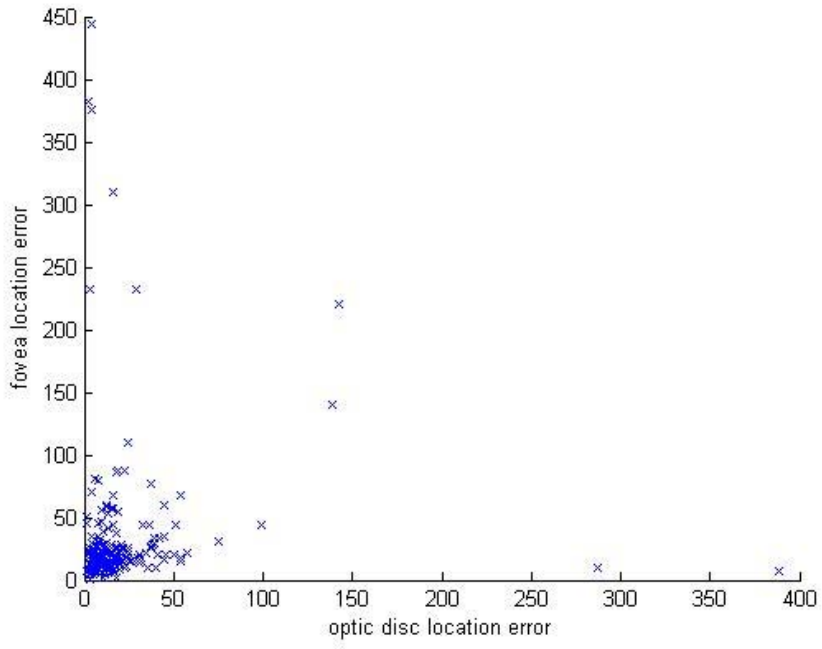

Figure 5.8: The correlated error of the optic disc and fovea for the right eye images. The x-axis is the distance error of the optic disc. The y-axis is the corresponding distance error of the fovea.

The mean distance error and standard deviation of the fovea for the right eye is 31.18 pixels and 51.1 pixels. 96.6% estimated results fall in a circle with a radius

www.manaraa.com

of $\mathcal{R} = 100$ centered at the true location. 87.9% estimated results fall in a circle with a radius of $\mathcal{R} = 50$ centered at the true location. The histogram of the distance error for the right eye is shown in Fig. 5.4.

The correlated error is shown in Fig. 5.8. The figure shows the distance error of the optic disc and fovea of the same image together. Most of the images have a correlated distance error within the 50 pixel -50 pixel rectangular. We can also see that the fovea detection is a little bit worse than the optic disc detection.

Fig. 5.7 shows all the detected location on one image. The true locations of the optic discs have been registered to the true location of the optic disc of this given image. The true locations of the foveae have been registered to the true location of the fovea of this given image as well.

www.manaraa.com

CHAPTER 6
DISCUSSION

6.1 Advantages of Proposed Method

Method proposed in this thesis has several improvements comparing with previous work. First of all, the first stage of the detection is a simultaneous but independent detection of the optic disc and the fovea. The conventional way to detect both optic disc and fovea is to first detect the optic disc using some algorithm, and then detect the fovea depending on the result of the optic disc detection [6] [10] [19] [20]. The fovea detection could not provide any feedback to the optic disc detection. Our method achieves the independent but simultaneous detection of the optic disc and fovea using the same set of features.

Secondly, we then introduce the mutual information between the two structures to enhance the result. During the enhancement, the fovea detection is not depend on the optic disc detection. Neither does the optic disc detection depend on the fovea detection. One structure is just given the right to adjust the detection of the other structure by putting more weight to the place that it believes to be the true location of the other structure. If the other structure is in an expected location, its probability of being the true location gets even higher. If it is not in an expected location, whether or not the algorithm accept this adjustment depends on the comparison between the originally detected location from the first stage and the enhanced location from the second stage. If the original detected location gives a stronger indication (i.e. higher probability) than the enhanced location from the second stage, the estimated location remains unchanged. On the other hand, if the

www.manaraa.com

enhanced location gives a stronger indication, the estimated location will move to the location suggested in the second stage.

Thirdly, new features are introduced for the classification. Features from the distance transform image, such as the average distance to the nearest blood vessel and maximum distance to the nearest blood vessel, were not used in previous work. We also tried to extract features from the red, green and blue channels. The feature selection result proves that the green channel contains more information than the other two channels on a color fundus photograph.

6.2 Factors that Influence the Results

6.2.1 Vessel Probability Image

As mentioned in Section 3.1, the image preprocessing includes getting the vessel probability images. Blood vessel features is actually a very important part of the feature set. Hence the quality of the vessel probability image will greatly influence the optic disc and fovea detection results. In other words, if the vessel probability image contains insufficient information, the detection result will be influenced largely.

Fig 6.1 shows some example vessel probability images and the optic disc and fovea detection results. The top row shows what a normal vessel probability image looks like and the corresponding optic disc/fovea probability image. The second row and last row show two bad cases where insufficient information is provided by the vessel probability image. Not surprisingly, the optic disc/fovea probability image is completely devastated. However, these results are actually very reasonable because the absence of vessel, i.e. low vessel density, is a very important property of the fovea area. That is why a large region is labeled dark if the vessel image implies so.

www.manaraa.com

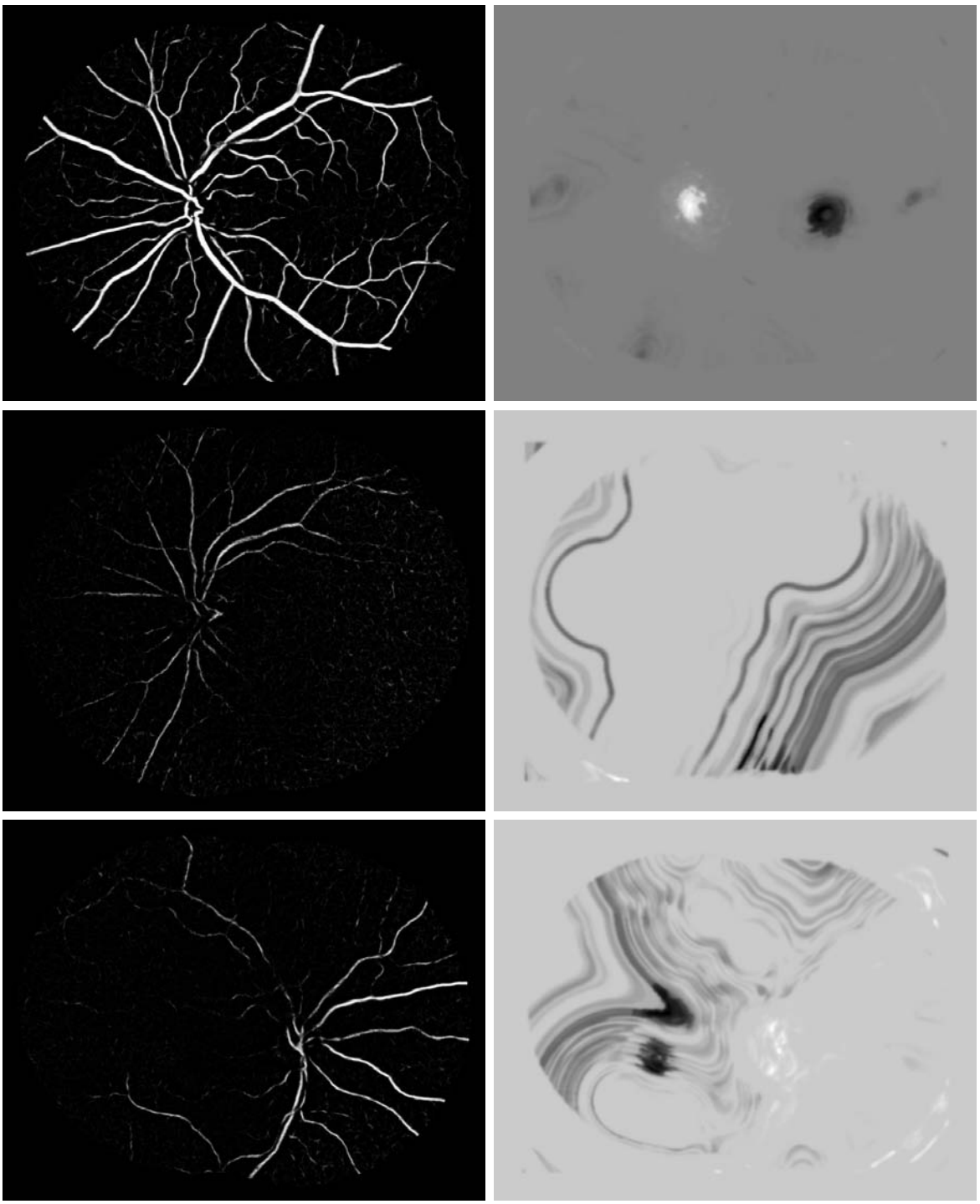

Figure 6.1: The effect of vessel probability image on the detection result. The top row shows what a normal vessel probability image looks like and the corresponding optic disc/fovea probability image. The second row and last row show two bad cases where insufficient information is provided by the vessel probability image.

www.manaraa.com

6.2.2 Image Quality

The image quality will effect the detection result greatly. If severe diseases or flaws appear on the image, it will influence the result. Our method is capable of handle some of the low quality images or images with severe diseases. Fig. 6.2 shows some cases with low quality images and their result.

But there are also cases that our method fails to detect the correct locations on the low quality images. Some examples are shown in Fig. 6.3.

6.3 Future Work

Future work will be focused on several aspects. First, the vessel probability image needs to be improved. As discussed in Section 6.2, the vessel probability image is one of the important feature source. Its quality will influence the final result to a great extent.

Another important aspect is the improvement of the features in the first k-NN classification. Though the second k-NN classification is a nice way to improve and correct the result of the first k-NN classification, it will of course be better if we don't need this corrections. Moreover, second k-NN would not help much if the first k-NN result is too bad.

A last thing need to be considered is the improvement of running time. Currently, it takes $\pm$20min to run one test image. If we want to put this method into use, the running time needs to be improved. A possible way is to calculate probabilities for every other pixels and then do the intensity interpolation, in stead of running every pixel on the test image. Another possible way is to decrease feature number and optimize feature computation.

www.manaraa.com

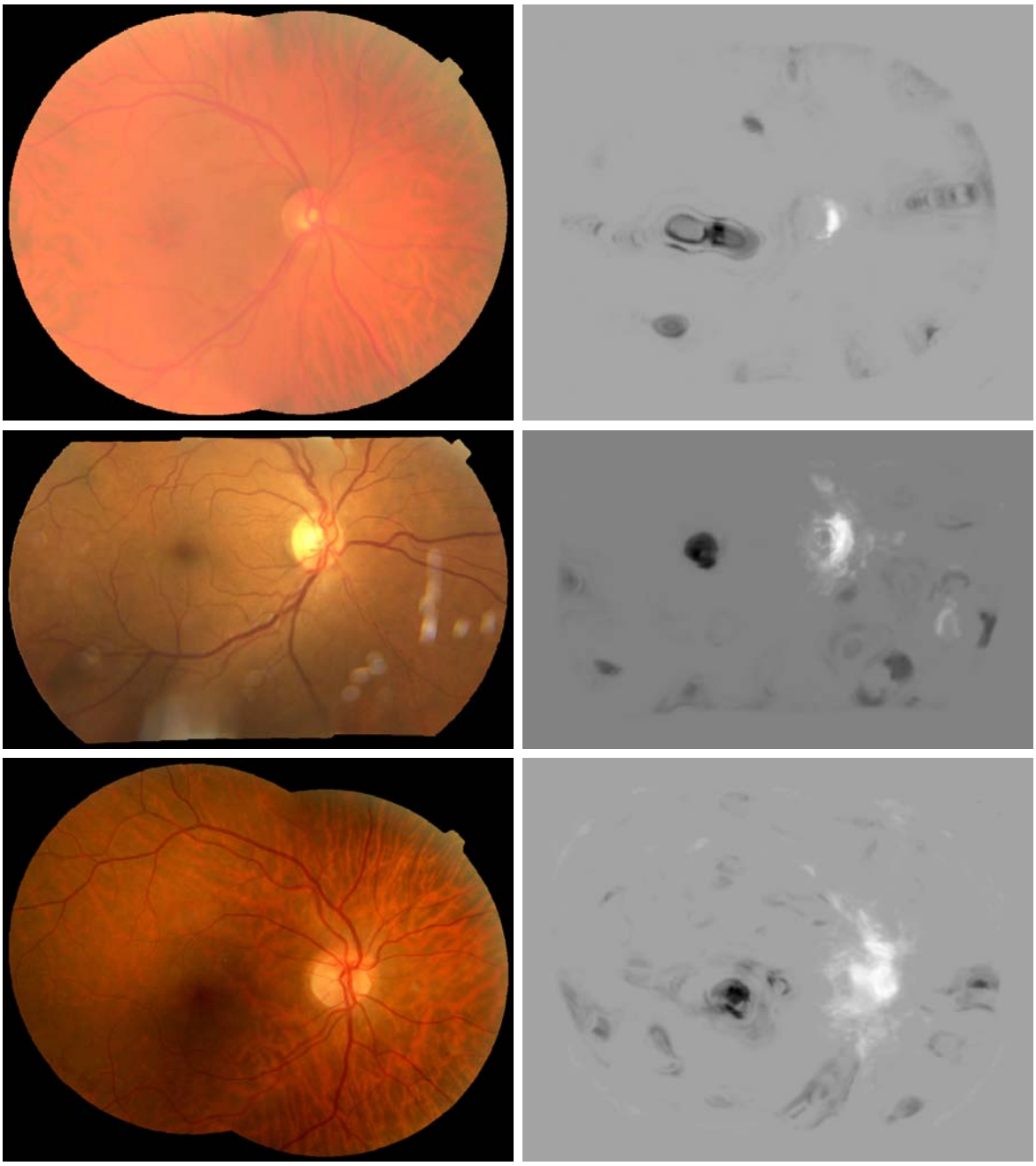

Figure 6.2: Examples of bad quality fundus images and results. The left column shows the fundus images. The right column shows the optic disc/fovea detection results. Though the image qualities are low, our system is able to correctly detect the locations.

www.manaraa.com

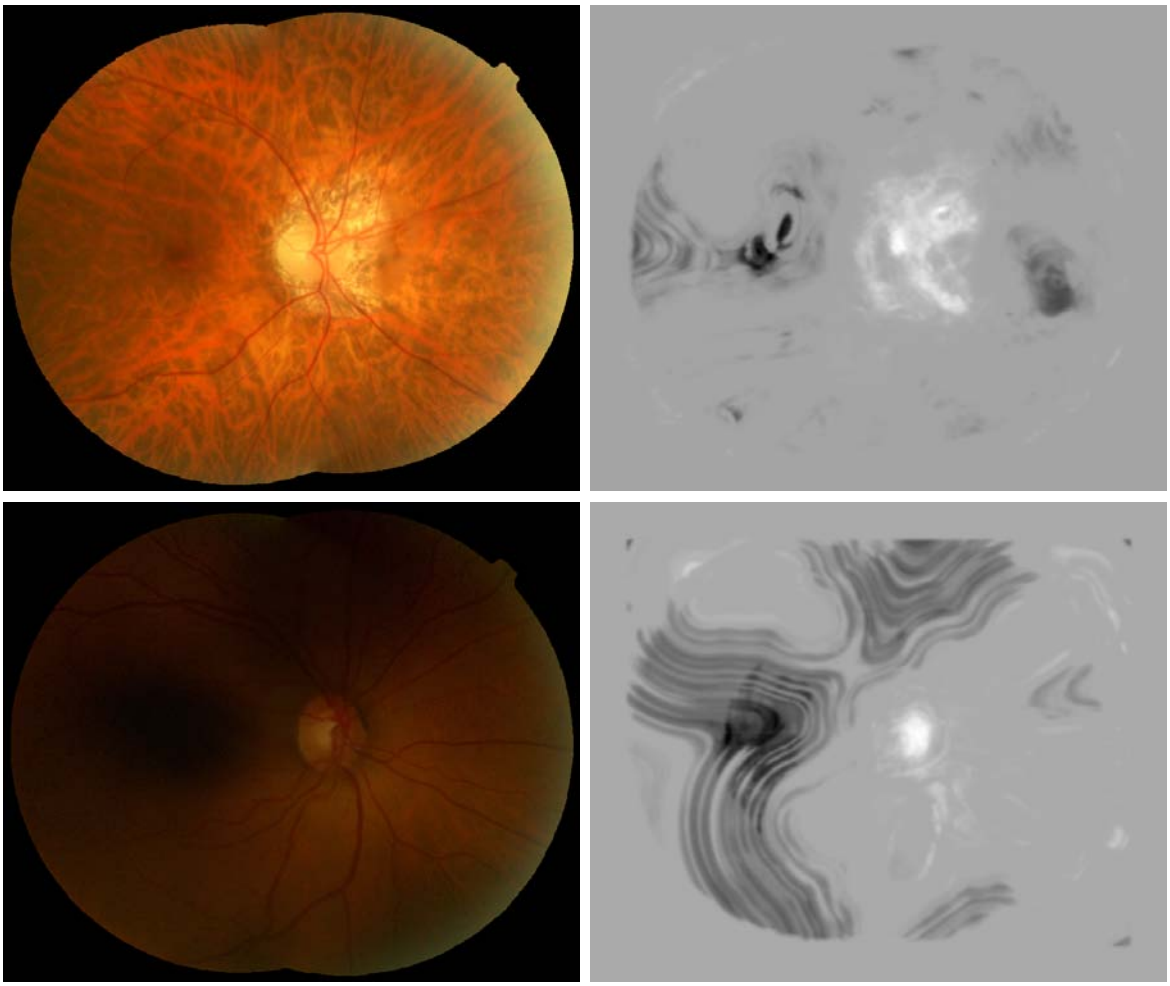

Figure 6.3: Examples of bad quality fundus images and results. The left column shows the fundus images. The right column shows the results. Our system failed to detect the optic disc/fovea locations.

www.manaraa.com

CHAPTER 7
CONCLUSION

We proposed an automatic and simultaneous detection method for optic disc and fovea on color fundus image in this study. Specifically, we introduced an enhancement and correction step, which allows the detection result of one structure to facilitate the detection of the other one. In the first step of the method, a set of features are extracted from the color fundus image, and the relationship between the feature set and a distance variable d is established during training phase. Then for a test image, the same set of features is measured and the distance to the optic disc and fovea can be estimated using k-NN classification. A probability image with every pixel labeled a probability of within an optic disc or a fovea is generated during this step. In the second step of the method, a second k-NN classification is applied on the probability image. Information like intensity, distance and angle between the two structures are extracted and trained. Then for a test image, detected high likelihood regions from the first step can be enhanced only if they satisfy the trained relationship. The detected regions that do not get support from the other detected structure will be suppressed.

We tested this method and the results shows high accuracy. This method is capable of handling some bad cases with low image quality or severe diseases. This is a fully automatic method to detect the optic disc and fovea simultaneously with excellent performance.

www.manaraa.com

REFERENCES

[1] Cjroyle opticians: Fundus camera. http://www.cjroyleopticians.co.uk/html/services.html.

[2] National eye institute: cataracts. http://www.nei.nih.gov/health/cataract/.

[3] National eye institute: glaucoma. http://www.nei.nih.gov/health/glaucoma/.

[4] visual system: light path. http://www.avalonfalling.com/?m=200902.

[5] Micheal D. Abramoff and Stephen R. Russell. Improving diabetic eye care-telediagnosis studies show promise for this large patient population. *Ophthalmology Management*, 2006.

[6] A.D.Fleming, K.A.Goatman, S.Philip, J.A.Olson, and P.F.Sharp. Automatic detection of retinal antomy to assist diabetic retinopathy screeing. *Physics in Medicine and Biology*, 52:331–345, 2007.

[7] Eyes and Eyesight. anatomy of the eye. http://www.eyesandeyesight.com /2009/02 /anatomy-of-the-eye/.

[8] M. Foracchia, E. Grisan, and A. Ruggeri. Detection of optic disc in retinal images by means of a geometrical model of vessel structure. *IEEE Transactions on Medical Imaging*, 23(10):1189–1195, 2004.

[9] Adam Hoover and Michael Goldbaum. Locating the optic nerve in a retinal image using the fuzzy convergence of the blood vessel. *IEEE Transactions on Medical Imaging*, 22(8):951–958, 2003.

[10] Huiqi Li and Opas Chutatape. Automated feature extraction in color retinal images by a model based approach. *IEEE Transaction on Biomedical Engineering*, 51(2):246–253, 2004.

[11] James Lowell, Andrew Hunder, David Steel, Ansu Basu, Robert Ryder, and Eric Fletcher. Optic nerve head segmentation. *IEEE Transaction on Medical Imaging*, 23:256–264, 2004.

[12] M.Sonka, V.Hlavac, and R.Boyle. *Image Processing, Analysis, and Machine Vision*. PWS, New York, 1998.

[13] M. Niemeijer, M.D.Abramoff, and B. van Ginneken. Automated localization of the optic disc and the fovea. *IEEE EMBS Conference*, pages 3583–3541, 2008.

www.manaraa.com

[14] M. Niemeijer, J. Staal, B. van Ginneken, M. Loog, , and M.D.Abramoff. Comparative study of retinal vessel segmentation methods on a new publicly available database. *SPIE Medical Imaging*, 5370:648–656, 2004.

[15] Meindert Niemeijer. *Automatic Detection of Diabetic Retinopathy in Digital Fundus Photographs*. 2006.

[16] P. Pudil, F.J. Ferri, J. Novovicova, and J. Kittler. Floating search methods in feature selection. *Pattern Recognition Letters*, 15(11):1119–1125, 1994.

[17] Anthony S. Robbins, Leo D. Hurley, Eric J. Dudenhoefer, and Susan Y. Chao. Performance characteristics of digital fundus photography as a screening test for diabetic retinopathy in a low-risk population. *Diabetes Technology and Therapeutics*, 3(2):193–200, 2001.

[18] Laurelee Sherwood. *Human Physiology-From Cell to Systems*. Jack Carey, 2001.

[19] C. Sinthanayothin, J. Boyce, H. Cook, and T. Williamson. Automated localisation of the optic disc, fovea, and retinal blood vessels from digital colour fundus images. *British Journal of Ophthalmology*, 83(11):902–910, 1999.

[20] K. Tobin, E. Chaum, V. Govindasamy, and T. Karnowski. Detection of anatomic structures in human retinal imagery. *IEEE Transaction on Medical Imaging*, 26(12):1729–1739, 2007.

www.manaraa.com